Calculating the spin memory loss at Cu|metal interfaces from first principles

Ruixi Liu,[1] Kriti Gupta,[2] Zhe Yuan,[1,*] and Paul J. Kelly[1,2,†]

[1]*Center for Advanced Quantum Studies and Department of Physics, Beijing Normal University, 100875 Beijing, China*

[2]*Faculty of Science and Technology and MESA+ Institute for Nanotechnology, University of Twente, P.O. Box 217, 7500 AE Enschede, The Netherlands*

(Received 14 March 2022; revised 22 June 2022; accepted 22 June 2022; published 5 July 2022)

The role played by interfaces in metallic multilayers is not only to change the momenta of incident electrons; their symmetry lowering also results in an enhancement of the effects of spin-orbit coupling, in particular, the flipping of the spins of conduction electrons. This leads to a significant reduction of a spin current through a metallic interface that is quantitatively characterized by a dimensionless parameter δ called the spin memory loss (SML) parameter, the interface counterpart of the spin-flip diffusion length for bulk metals. In this paper, we use first-principles scattering calculations that include temperature-induced lattice and spin disorder to systematically study three parameters that govern spin transport through metallic interfaces of Cu with Pt, Pd, Py (permalloy), and Co: the interface resistance, spin polarization, and the SML. The value of δ for a Cu|Pt interface is found to be comparable to what we recently reported for a Au|Pt interface [Gupta *et al.*, Phys. Rev. Lett. **124**, 087702 (2020)]. For Cu|Py and Cu|Co interfaces, δ decreases monotonically with increasing temperature to become negligibly small at room temperature. The calculated results are in good agreement with currently available experimental values in the literature. Inserting a Cu layer between Pt and the Py or Co layers slightly increases the total spin current dissipation at these compound interfaces.

DOI: 10.1103/PhysRevB.106.014401

I. INTRODUCTION

Since the discovery of giant magnetoresistance (GMR) in magnetic multilayers [1–3], interfaces have been recognized to play an essential role in the observation of many spintronics phenomena including spin-transfer torque [4–11], the spin Hall effect (SHE) [12–18], spin pumping [19–25], the spin Seebeck effect [26–28], etc. In particular, the flux of spin angular momentum carried by a spin-polarized current of electrons or by a pure spin current may be significantly reduced at an interface. This loss of spin flux [29] is described in terms of a dimensionless parameter δ called the spin memory loss (SML) [30] and is confirmed in many experimental studies [31–33]. When spin-transport parameters such as the spin Hall angle and the spin-flip diffusion length (SDL) are being evaluated [34–39], it becomes critically important to know its numerical value. Neglecting it can lead to severely underestimated values of the SDL l_{sf}, which in turn influences the estimated values of the spin Hall angle [24,40–42].

In semiclassical transport theory [43], the transport of a current of spins through an interface is described in terms of an interface resistance AR_{I} and the spin asymmetry γ, as well as the SML δ. The main way in which these interface parameters are determined is by measuring the GMR in a so-called current-perpendicular-to-the-plane (CPP) configuration. This technique is limited by the small value of the interface resistance between two metals (and its spin dependence) compared to those of typical leads. This problem can be overcome by reducing the sample cross section [44] or by using superconducting leads [45]. At the low temperatures dictated by the superconducting transition temperatures of lead materials like Al or Nb, transport is dominated by disorder, such as interface roughness about which little is usually known for specific samples. Studies based on first-principles scattering theory can model many types of interface disorder [8,46–49] as well as temperature-induced bulk disorder [50] and thereby shed light on the SML and its relationship with microscopic scattering mechanisms [51]. A number of theoretical studies of the SML have recently been reported for interfaces between nonmagnetic (NM) materials [51–53] and between ferromagnetic (FM) and NM materials [51,54–56] with a strong focus on interfaces between the transition metal Pt and another metal.

Pt is an important NM metal in spintronics because of its large spin-to-charge conversion efficiency. It is widely used to generate spin currents via the SHE and to detect spin currents via its inverse, the ISHE. Pt (and Pd) have very high densities of states at the Fermi energy and are relatively easily magnetized [57,58] by proximity to a magnetic material [59,60]. To avoid this happening while incurring minimal attenuation of the spin current, a thin Cu spacer layer is frequently inserted between Pt and magnetic materials [61–63], making it of interest to study such compound interfaces. Because of its long SDL that is estimated to be hundreds of nanometers at room temperature [33], Cu is widely used in nonlocal spin valves as a transport channel for a diffusive spin current [37,64–69]. In such studies, the important interfaces are Cu|NM

*zyuan@bnu.edu.cn

†P.J.Kelly@utwente.nl

and Cu|FM interfaces where NM is usually Pt or Pd and FM is Py (permalloy, $Ni_{80}Fe_{20}$) or Co. Because of the difficulty of estimating the SML at interfaces involving Cu, it is often simply neglected.

In this paper, we present a systematic study of the transport parameters AR_I, γ, and δ for interfaces comprising Cu and Pd, Pt, Co, and Py using first-principles relativistic scattering calculations [70] that take into account temperature-induced lattice and spin disorder [50] as well as alloy disorder [71] and lattice mismatch [40,51,56]. The SML parameters for Cu|Py and Cu|Co interfaces are found to decrease monotonically with increasing temperature and become negligibly small at room temperature. Inserting a thin Cu layer between Pt and Py or Co layers increases the total spin current reduction at the compound Pt|Cu|FM interface slightly because of the nonnegligible SML at the Cu|Pt interface.

The rest of this paper is organized as follows. In Sec. II, we briefly summarize the theoretical methods and provide some technical details of the calculations. The main results are presented and discussed in Sec. III, where we begin by estimating the SDL of Cu, which must be known before we calculate the SML for Cu|metal interfaces. This is followed by the results for Cu|Pt, Cu|Pd, Cu|Py, and Cu|Co interfaces and their dependence on temperature and interface atomic mixing. A brief summary is given in Sec. IV. In the Appendix, the formalism required to determine the SML for NM|FM interfaces using a bilayer structure is derived and it is shown to yield the same results for Pt|Py interface parameters as were obtained for a Pt|Py|Pt trilayer in Ref. [56].

II. THEORETICAL METHODS AND COMPUTATIONAL DETAILS

Most transport experiments in the field of spintronics are interpreted in terms of parameters that are defined in semiclassical transport theory [43]. A typical example is the Valet-Fert model which is used to describe the results of CPP-MR experiments [72,73] using the bulk transport parameters ρ (resistivity), β (conductivity asymmetry), and l_{sf} (SDL) together with the corresponding three interface parameters AR_I, γ, and δ. While the calculation of bulk transport parameters using first-principles scattering theory has already been documented [42,70], determining the interface parameters is less trivial. In this section, we present the formulation [51] that we use to extract the parameters from the first-principles calculations when combined with a layer-averaged local current scheme [42]. Further details of the formulation are provided elsewhere [56,74]. The results of semiclassical transport theory that we will need are summarized in Sec. II A. They are applied to an NM|NM′ interface in Sec. II B and to an FM|NM interface in Sec. II C. Some technical details of the calculations are given in Sec. II D.

A. Spin diffusion equation

In an axially symmetric layered structure, the current flow in the z direction, perpendicular to the interfaces, is described by the spin diffusion equation [43],

$$\frac{\partial^2 \mu_s}{\partial z^2} = \frac{\mu_s}{l_{sf}^2}, \tag{1}$$

where l_{sf} represents the SDL and μ_s is the spin accumulation defined as the difference between the spin-up and spin-down chemical potentials, $\mu_s = \mu_\uparrow - \mu_\downarrow$. The spin-dependent chemical potential $\mu_{\uparrow(\downarrow)}$ drives the corresponding current density $j_{\uparrow(\downarrow)}$ according to Ohm's law,

$$j_{\uparrow(\downarrow)}(z) = -\frac{1}{e\rho_{\uparrow(\downarrow)}} \frac{\partial \mu_{\uparrow(\downarrow)}}{\partial z}, \tag{2}$$

where $\rho_{\uparrow(\downarrow)}$ is the spin-dependent bulk resistivity and it is assumed that the two spin channels are weakly coupled. The general solutions of Eqs. (1) and (2) are

$$\mu_s(z) = Ae^{z/l_{sf}} + Be^{-z/l_{sf}} \tag{3}$$

and

$$j_{\uparrow(\downarrow)}(z) = \frac{1 \pm \beta}{2} j \mp \frac{1-\beta^2}{4e\rho l_{sf}} (Ae^{z/l_{sf}} - Be^{-z/l_{sf}}), \tag{4}$$

respectively, where the coefficients A and B are determined by appropriate boundary conditions. Here $\beta = (\rho_\downarrow - \rho_\uparrow)/(\rho_\uparrow + \rho_\downarrow)$ is the bulk spin asymmetry, $j = j_\uparrow + j_\downarrow$ denotes the total current density, and ρ is the total resistivity given by $\rho^{-1} = \rho_\uparrow^{-1} + \rho_\downarrow^{-1}$. We define the normalized spin-current density to be $j_s = (j_\uparrow - j_\downarrow)/(j_\uparrow + j_\downarrow)$, which can be written as

$$j_s(z) = \beta - \frac{1-\beta^2}{2ej\rho l_{sf}} (Ae^{z/l_{sf}} - Be^{-z/l_{sf}}). \tag{5}$$

Equation (5) can be used together with the spin current density calculated from first principles to extract β and l_{sf} [42], while ρ is determined independently from the scattering matrix using the Landauer formula [70].

B. NM|NM′ interfaces

For a NM metal or alloy with an equal number of spin-up and spin-down electrons, $\rho_\uparrow = \rho_\downarrow = 2\rho$, $\beta = 0$, and Eq. (5) simplifies to

$$j_s(z) = \frac{1}{2ej\rho l_{sf}} (Be^{-z/l_{sf}} - Ae^{z/l_{sf}}). \tag{6}$$

If a fully polarized spin current is injected from an artificial half-metallic left lead ($z \leqslant 0$) into a diffusive NM|NM′ bilayer so $j_s(0) = 1$, then the spin current will decay in both NM metals and, provided the bilayer is sufficiently thick, will vanish at the right lead, $j_s(\infty) = 0$. On each side of the interface, Eq. (6) can be used to fit the calculated $j_s(z)$ to obtain the corresponding SDL $l_i \equiv l_{sf}^i$ for each metal, $i =$ NM, NM′. Extrapolation of the fitting curves to the interface yields two different values for the spin current at the interface, $j_s(z_I - \eta) \neq j_s(z_I + \eta)$, where η is a positive infinitesimal. The corresponding discontinuity, shown in Fig. 3, represents the interface SML.

In the absence of appropriate boundary conditions for a NM|NM′ interface, we follow Refs. [24,32,33,40] and model the interface (I) as a fictitious bulklike material with a finite thickness t, a resistivity ρ_I and SDL l_I. By doing so, the NM|NM′ bilayer becomes a NM|I|NM′ trilayer in which the spin current and spin accumulation are everywhere continuous. Taking the limit $t \to 0$, we recover the conventional

interface resistance AR_I as well as the SML δ,

$$AR_I = \lim_{t\to 0} \rho_I t; \quad \delta = \lim_{t\to 0} t/l_I, \tag{7}$$

where the cross-sectional area A should not be confused with the disposable constant in Eq. (6). In this way, the discontinuity at the interface is naturally included in the semiclassical spin diffusion theory. The result of imposing continuity on μ_s and j_s and then taking the limit $t \to 0$ is

$$\frac{j_s(z_I - \eta)}{j_s(z_I + \eta)} = \cosh\delta + \frac{\rho_{NM'} l_{NM'}}{AR_I}\,\delta \sinh\delta. \tag{8}$$

By calculating the bulk parameters $\rho_{NM'}$ and $l_{NM'}$ and the interface resistance AR_I independently, only the single unknown parameter δ needs to be determined from Eq. (8), which can be straightforwardly solved numerically. The calculation of AR_I using the Landauer-Büttiker formalism will be presented in Sec. III B.

C. FM|NM interfaces

Unlike NM metals for which $\beta = 0$, the asymmetry between the spin-up and spin-down conducting channels in a FM metal leads to β saturating to a finite value well inside the ferromagnet, on a length scale of l_{sf}. We therefore construct a symmetric NM|FM|NM trilayer with the origin $z = 0$ at the center of the FM layer and inject an electric current from a NM lead imposing the boundary conditions $j_s(-\infty) = j_s(\infty) = 0$. The calculated spin current in the FM metal can be fitted using Eq. (5) to extract β, l_{FM} [42] and $j_s(z_I - \eta)$ [51,56]. In the NM metal, the fitting using Eq. (6) is still applicable, resulting in l_{NM} and $j_s(z_I + \eta)$ where, because of the symmetry and without loss of generality, we just consider the rightmost FM|NM interface. Just as we did for the NM|NM′ interface, we transform the FM|NM interface into an FM|I|NM trilayer with a finite thickness t of the interface region. The only difference is that the FM|NM interface resistance is spin dependent and the parameter $\gamma \equiv (AR_\downarrow - AR_\uparrow)/(AR_\uparrow + AR_\downarrow)$ is introduced to characterize the spin polarization.

Taking the limit $t \to 0$ yields the interface discontinuity $j_s(z_I - \eta) - j_s(z_I + \eta) \neq 0$ and the analysis [56] results in two implicit equations,

$$j_s(z_I - \eta) = \gamma - \frac{(1-\gamma^2)\delta}{AR_I \sinh\delta}\left\{\rho_{NM} l_{NM}\, j_s(z_I + \eta) - \cosh\delta \frac{\rho_{FM} l_{FM}}{1-\beta^2} \tanh\left(\frac{z_I}{l_{FM}}\right)[\beta - j_s(z_I - \eta)]\right\}, \tag{9a}$$

$$j_s(z_I + \eta) = \gamma - \frac{(1-\gamma^2)\delta}{AR_I \sinh\delta}\left\{\rho_{NM} l_{NM}\, j_s(z_I + \eta)\cosh\delta - \frac{\rho_{FM} l_{FM}}{1-\beta^2} \tanh\left(\frac{z_I}{l_{FM}}\right)[\beta - j_s(z_I - \eta)]\right\}, \tag{9b}$$

which can be solved to yield the remaining unknown variables δ and γ [51,56].

The boundary conditions $j_s(-\infty) = j_s(\infty) = 0$ are appropriate for structures with NM materials like Pt, for which l_{sf} is short, embedded between NM leads [56]. When l_{sf} is as long as it is for NM=Cu, it is not possible to treat a thickness of the NM metal so large that the spin current can be assumed to have decayed to zero at the interfaces with the leads. Instead, we consider the injection or detection of a spin-polarized current corresponding to the boundary conditions $j_s(-\infty)$ or $j_s(\infty)$ equal to the current polarization P which can have an arbitrary value in the range $[-1, 1]$. For simplicity, a half-metallic FM lead is considered in the Appendix, where $j_s(-\infty) = \pm 1$ is explicitly illustrated. Within the accuracy of the calculations, both sets of boundary conditions lead to the same interface parameters.

D. Computational details

Our starting point is an electronic structure for the layered metallic system of interest, calculated self-consistently within the framework of density functional theory [75,76]. The electronic wave functions are expanded in terms of tight-binding linearized muffin-tin orbitals [77] in the atomic spheres approximation [78]. We use the local density approximation with the exchange-correlation functional parameterized by von Barth and Hedin [79]. Transport is addressed by solving the quantum mechanical scattering problem for a general two-terminal geometry using Ando's wave-function matching method [80] implemented [49,81] with the tight-binding muffin-tin orbital basis. The conductance is calculated directly from the scattering matrix for the scattering region embedded between semi-infinite ballistic leads [82]. The full quantum-mechanical wave functions are explicitly determined throughout the scattering region from which we calculate position-dependent charge and spin currents [42,83]. Spin-orbit coupling was neglected in calculating the self-consistent atomic potentials but included in the transport calculations [70].

Temperature-induced lattice and spin disorder, alloy disorder, and lattice mismatch can be efficiently modeled in lateral supercells that assume a measure of periodicity in the directions transverse to the transport direction [42,70]. The lattice constant of Pt is $a_{Pt} = 3.924$ Å, that of Pd just 0.8% smaller, $a_{Pd} = 3.891$ Å [84]. Those of Py, Co, and Cu are about 10% smaller but quite similar with $a_{Py} = 3.541$ Å [70], $a_{Co} = 3.539$ Å [85], and $a_{Cu} = 3.615$ Å [84]. For the Cu|Pt, Cu|Pd, Py|Pt, and Co|Pt interfaces studied here, an 8×8 interface unit cell of (111) Cu, Py, or Co is chosen to match to a $2\sqrt{13} \times 2\sqrt{13}$ interface unit cell of Pt or Pd (neglecting the 0.8% difference), which allows all materials to be kept fcc. The two-dimensional Brillouin zone of the 8×8 supercell of (111) Cu is sampled using 28×28 k points and the same k mesh density is used for all the transport calculations. Py is chosen to have its equilibrium lattice constant. To study Cu|Py and Cu|Co interfaces, Cu must be compressed slightly to

match Py, respectively, Co; as shown for Au in Refs. [74,85], this changes the Fermi surface and hence the transport properties of the noble metal negligibly. The alloy disorder of bulk Py is modeled by randomly populating lateral supercell sites with Fe and Ni atomic sphere potentials subject to the required stoichiometry [70], where the atomic potentials of the alloy are calculated self-consistently within the coherent potential approximation [86,87]. Interface disorder arising from interface mixing (see Sec. III D) is modeled as a number of layers of interface alloy [8,46–49,51,74].

Temperature-induced disorder is modeled in the adiabatic approximation using a frozen thermal lattice disorder scheme with atoms displaced at random from their equilibrium lattice positions with a Gaussian distribution of displacements. The root mean square displacement Δ characterizing the distribution is chosen so the resistivity of the NM metal at a finite temperature is reproduced as detailed in Ref. [50]. For example, we need a value of $\Delta = 0.021 a_{\mathrm{Cu}}$ to reproduce the room-temperature resistivity of bulk Cu, 1.8 $\mu\Omega$ cm. This value of Δ may be compared to values obtained by populating phonons at 300 K ($0.027 a_{\mathrm{Cu}}$) [50] from room temperature molecular dynamics simulations ($0.023 a_{\mathrm{Cu}}$) [88] or from 160 K x-ray diffraction measurements ($0.018 a_{\mathrm{Cu}}$) [89]. For a FM metal, not only are the atom positions influenced by temperature but also their magnetic ordering. We use a simple Gaussian model of spin disorder parameterized to reproduce the experimental magnetization of the ferromagnet at a given temperature, combined with lattice disorder so together they reproduce the experimental resistivity as discussed in Refs. [50,70]. This spin disorder is equivalent to the Fisher distribution [90] at low temperature when the tilting angle measured from the global quantization axis is small [70]. The numerical convergence has been extensively examined with respect to the maximum angular momentum in the basis, size of the lateral supercell, k-mesh sampling of the two-dimensional Brillouin zone, the number of random configurations of lattice and spin disorder, as well as the influence of the three-center integrals in the spin-orbit interaction [42,56,70,74]. Compared to calculations of the conductance, we find that more configurations are needed to reduce the error bars on the local currents to acceptable levels.

III. RESULTS AND DISCUSSION

Before we calculate the SML for Cu|metal interfaces, the SDL of bulk Cu is estimated in Sec. III A. Cu|Pt and Cu|Pd interfaces are considered in Sec. III B, followed by Cu|Py and Cu|Co interfaces in Sec. III C. The effect of interface atomic mixing for materials with similar atomic volumes is examined in Sec. III D for Cu|Co and Cu|Py interfaces. A compound interface obtained by inserting atomic layers of Cu between FM and Pt is studied in Sec. III E.

A. Estimating l_{Cu}

In the semiclassical theory commonly used to describe spin transport, five bulk parameters ρ_{NM}, l_{NM}, ρ_{FM}, l_{FM}, β, and three interface parameters AR_{I}, δ, and γ are required to describe transport through the FM|NM interface of a bilayer, while the bulk and interface spin polarizations β and γ vanish for an interface between two NM metals. The numerical techniques required to determine the resistivity of a NM or FM metal, as well as the SDL of most transition metals and alloys using scattering theory are well documented [40,42,50,70]. For free-electron-like metals like Cu, Ag, and Au, l_{sf} may be as large as several hundred nanometers to micrometers and a quantitative estimation requiring the length of the scattering region to be longer than 3-4 $\times\, l_{\mathrm{sf}}$ becomes computationally very demanding [91]. To estimate l_{Cu}, we therefore calculated ρ_{Cu} and l_{Cu} simultaneously at elevated temperatures, as a function of the root-mean-square-displacement $\Delta(T)$, to determine the product $\rho(T) l_{\mathrm{sf}}(T)$ that for the Elliott-Yafet mechanism of spin relaxation should be temperature independent and then used the confirmed linear relationship to extrapolate l_{Cu} to the required lower temperature.

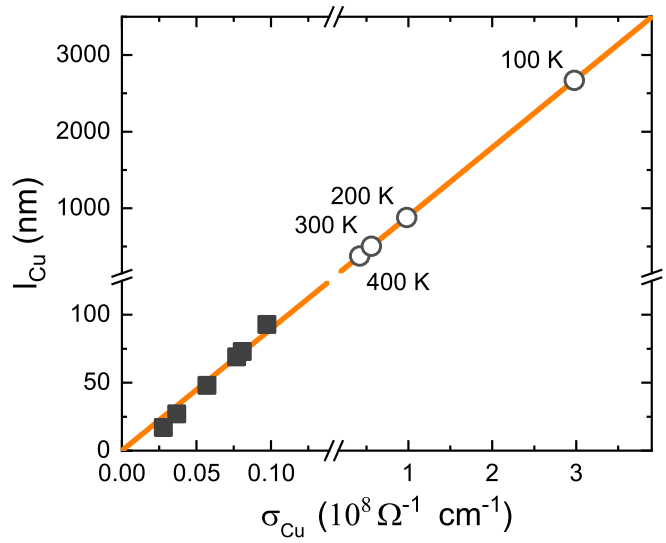

FIG. 1. Conductivity $\sigma_{\mathrm{Cu}} = 1/\rho_{\mathrm{Cu}}$ and corresponding spin diffusion length l_{Cu} at elevated temperatures (solid squares). The calculations were carried out using 8×8 lateral supercells perpendicular to the spin transport direction. Every point is averaged over 20 random configurations of thermal disorder. From the linear fit to a line that passes through the origin, we find the constant $\rho_{\mathrm{Cu}} l_{\mathrm{Cu}} = (9.0 \pm 1.0) \times 10^{-15}\ \Omega\ \mathrm{m}^2$, indicating that the Elliott-Yafet mechanism dominates the spin relaxation. Then the long spin-flip diffusion length at lower temperatures can be determined from the linear relationship using the documented resistivity of Cu at a given temperature (empty circles).

$l_{\mathrm{Cu}}(\Delta(T))$ is plotted in Fig. 1 as a function of the simultaneously determined conductivity for a number of values of Δ (solid squares); the approximate linearity indicates that the Elliott-Yafet mechanism [92,93] is dominant [91]. The product $\rho_{\mathrm{Cu}} l_{\mathrm{Cu}} = (9.0 \pm 1.0) \times 10^{-15}\ \Omega\ \mathrm{m}^2$ is obtained from linear least squares fitting. This linear relationship is extrapolated to the lower temperatures corresponding to the documented conductivity of bulk Cu at 100, 200, 300, and 400 K which are shown as the empty circles in Fig. 1. In particular, corresponding to the room temperature resistivity $\rho_{\mathrm{Cu}} = 1.8 \pm 0.1\ \mu\Omega$ cm, we estimate a value of $l_{\mathrm{Cu}} \sim 502$ nm.

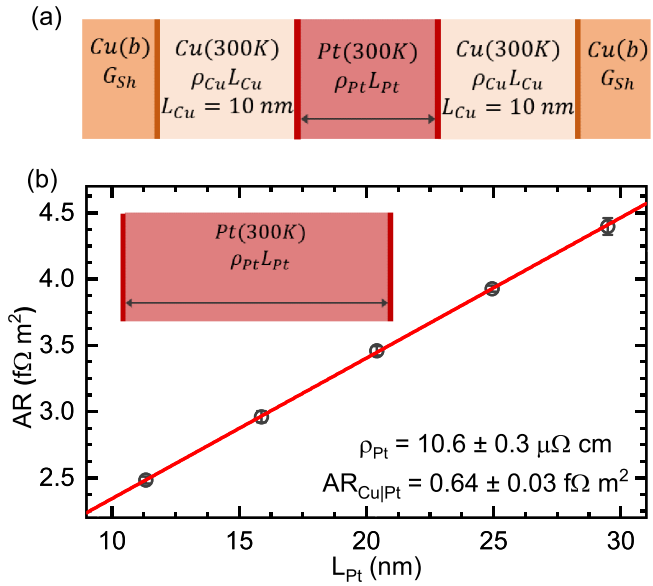

FIG. 2. (a) Schematic of the Landauer-Büttiker scattering geometry for a symmetric, diffusive Cu|Pt|Cu trilayer sandwiched between ballistic Cu leads. (b) Total resistance Eq. (10) of this geometry as a function of the Pt thickness L_{Pt} where the Sharvin conductance of the Cu leads, the interface resistance between the ballistic Cu leads and diffusive Cu, and the resistance of a length $2L_{Cu}$ of diffusive Cu have been subtracted leaving just $2AR_{Cu|Pt} + \rho_{Pt}L_{Pt}$. The data points at every thickness are the average of seven configurations of random thermal disorder. See the text for more details.

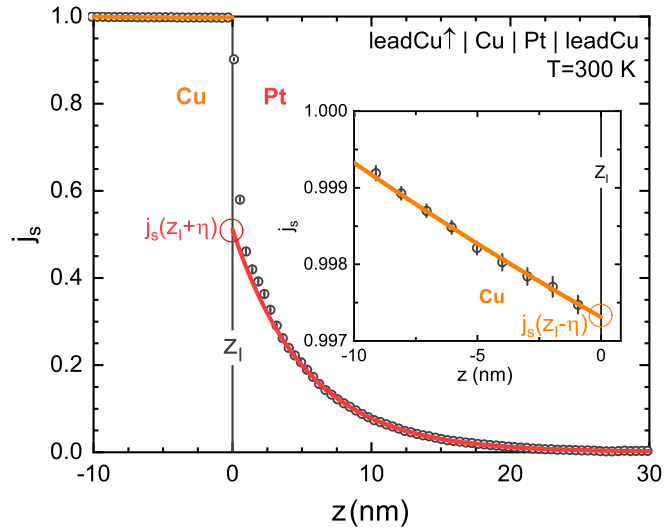

FIG. 3. Calculated spin current flowing through a diffusive Cu(10 nm)|Pt(30 nm) bilayer at 300 K, where a fully polarized spin current is injected from an artificial half-metallic Cu left lead. Averaged spin currents j_s are shown as grey circles. The error bars correspond to the root-mean-square deviation of twenty random configurations of thermal lattice disorder. The solid lines are fits using Eq. (6) in Cu (orange) and Pt (red), respectively. $j_s(z_I - \eta)$ and $j_s(z_I + \eta)$ indicate the values of the bulk spin currents extrapolated to the interface, z_I, from the Cu and Pt sides, respectively. Inset: Close-up of the spin current in the Cu layer.

B. Cu|Pt and Cu|Pd interfaces

We begin by examining the SML at the Cu|Pt interface that commonly appears in nonlocal spin-valve, spin-pumping, and spin-Seebeck experiments. We then compare our results when Pt is replaced by the isoelectronic and isostructural but lighter element Pd.

Before addressing the SML, the Cu|Pt interface resistance needs to be determined using the standard Landauer-Büttiker formalism [82,94]. As sketched in Fig. 2(a), we do this by sandwiching a symmetric, diffusive Cu|Pt|Cu trilayer between ballistic Cu leads in a two-terminal scattering configuration where element specific parameters Δ_i are used to reproduce the room-temperature resistivities of bulk Cu and Pt, respectively. The total calculated area resistance product for a cross-section A of the scattering geometry can be written as

$$AR_{\text{total}} = 1/G_{\text{Sh}} + 2AR_{\text{Cu|Lead}} + 2\rho_{\text{Cu}}L_{\text{Cu}} + 2AR_{\text{Cu|Pt}} + \rho_{\text{Pt}}L_{\text{Pt}}, \quad (10)$$

where G_{Sh} denotes the Sharvin conductance of the ballistic Cu leads, $AR_{\text{Cu|Lead}}$ is the resistance of the interface between the ballistic Cu lead and diffusive Cu, $2\rho_{\text{Cu}}L_{\text{Cu}}$ with $L_{\text{Cu}} = 10\,\text{nm}$ is the resistance of a length $2L_{\text{Cu}} = 20\,\text{nm}$ of diffusive Cu [95], $\rho_{\text{Pt}}L_{\text{Pt}}$ is the resistance of a length L_{Pt} of diffusive Pt, and $AR_{\text{Cu|Pt}}$ is the sought-after Cu|Pt interface resistance. By repeating the calculations without the central Pt layer, we obtain the contribution from the first three terms on the right-hand side of Eq. (10) separately. This is subtracted from the total resistance in Eq. (10), leaving us with $2AR_{\text{Cu|Pt}} + \rho_{\text{Pt}}L_{\text{Pt}}$ that is plotted in Fig. 2(b) as a function of L_{Pt} where each data point is obtained by averaging over seven configurations of random thermal disorder. The slope of the linear least-squares fit reproduces the resistivity of bulk Pt at room temperature while the intercept results in the interface resistance $AR_{\text{Cu|Pt}} = 0.64 \pm 0.03\,\text{f}\Omega\,\text{m}^2$.

l_{Pt} [42,91], l_{Cu}, and $AR_{\text{Cu|Pt}}$ have now been calculated, ρ_{Cu} and ρ_{Pt} have their experimental values by construction, leaving just $j_s(z_I + \eta)$ and $j_s(z_I - \eta)$ to be determined before $\delta_{\text{Cu|Pt}}$ can be evaluated using Eq. (8). To do so, we inject a fully polarized spin current from an artificial half-metallic Cu lead [42,70] into a diffusive, room temperature (RT: 300 K) Cu(10 nm)|Pt(30 nm) bilayer. The z-dependent spin current density is plotted in Fig. 3, where each data point corresponds to j_s averaged over an atomic layer and over 20 random configurations of thermal lattice disorder. On both sides of the interface, the spin current can be fitted very well using Eq. (6), as shown by the solid orange and red lines in Fig. 3. As expected from the large value of l_{Cu}, the spin current decays extremely slowly in Cu, as shown in the inset. To reduce the uncertainty from fitting, we use the room-temperature value $l_{\text{Cu}} \sim 502$ nm, yielding very good agreement with the calculated data. The spin current entering Pt exhibits an exponential decay which can be characterized by a value of $l_{\text{Pt}} = 5.3 \pm 0.1\,\text{nm}$ consistent with the value 5.26 ± 0.04 nm reported previously in Ref. [51]. The fitted semiclassical description of the spin current exhibits a substantial discontinuity at the Cu|Pt interface corresponding to the interface SML, Fig. 3. Using the values $j_s(z_I + \eta) = 0.997$ and $j_s(z_I - \eta) = 0.512$ obtained by extrapolation, $\rho_{\text{Pt}}l_{\text{Pt}} = 0.6\,\text{f}\Omega\,\text{m}^2$, and $AR_{\text{Cu|Pt}} =$

TABLE I. Spin memory loss δ for Cu|Pd, Cu|Pt, Au|Pd, and Au|Pt (111) interfaces. For Au|Pd and Au|Pt, we consider commensurate interfaces where Au is compressed so its lattice constant matches that of Pd/Pt and incommensurate, where the lattice mismatch between fully relaxed Au and Pd/Pt is accommodated using the large lateral supercells discussed in Sec. II D.

	Pd		Pt	
δ	Compressed	Relaxed	Compressed	Relaxed
Cu		0.45 ± 0.03		0.77 ± 0.04
Au [85]	0.43 ± 0.02	0.63 ± 0.02	0.62 ± 0.03	0.81 ± 0.05

$0.64 \pm 0.03\,\mathrm{f\Omega\,m^2}$, we finally estimate the SML to be $\delta_{\mathrm{Cu|Pt}} = 0.77 \pm 0.04$ for the Cu|Pt interface. This value of δ is very close to and only slightly smaller than the value of 0.81 we reported for the relaxed Au|Pt interface and substantially larger than the value 0.62 we found for the compressed Au|Pt interface [51], indicating the importance of taking lattice mismatch into account, Table I.

By repeating the complete procedure for the Cu|Pd interface and neglecting the 0.8% smaller lattice constant of Pd, we find $\delta = 0.45 \pm 0.03$ at 300 K that is smaller than the SML for the Cu|Pt interface because of the weaker spin-orbit interaction in Pd. This value for the Cu|Pd interface is also consistent with the SML values of 0.43 and 0.63 calculated for the commensurate (with Au compressed to match to Pd) and incommensurate Au|Pd interfaces [51], respectively. We attribute this agreement to the very similar electronic structures of Cu and Au, where the free-electron-like s band dominates transport at the Fermi level; the filled $3d$ or $5d$ bands are well below the Fermi energy so the difference in spin-orbit coupling strength between Cu and Au does not play a significant role.

We compare our calculated interface resistances and SML parameters with experimental and theoretical values available in the literature in Table II. For the Cu|Pt interface, our calculated values of AR_{I} and δ are somewhat smaller than the experimental values. Experimentally, the influence of temperature on the SML of a NM|NM′ interface is found to be weak [96], which is consistent with our theoretical findings [40,51]. This is because the main scattering mechanism at the interface is the abrupt variation in the atomic potentials experienced by conduction electrons [40]. For the Cu|Pd interface, the value we calculate for δ is in perfect agreement with that calculated by Belashchenko *et al.* [52] but is larger than the only reported, low-temperature experimental value [73]. To make more progress, structural properties need to be correlated with transport measurements. We identify a lack of structural characterization of interfaces on the atomic level as a major stumbling block to developing more comprehensive understanding. The theoretical description we have presented can be applied to considerably more complex structural models.

TABLE II. Experimental and calculated interface resistance AR_{I} and spin memory loss δ for Cu|Pt and Cu|Pd interfaces.

	$AR_{\mathrm{I}}(\mathrm{f\Omega\,m^2})$	δ	T(K)	Method	Ref.
Cu|Pt	0.75 ± 0.05	0.9 ± 0.1	4.2	CPP-MR	[73]
		0.95	7	CPP-MR	[96]
		0.89	295	CPP-MR	[96]
	0.64 ± 0.03	0.77 ± 0.04	300	This paper	
Cu|Pd	0.45 ± 0.05	$0.24^{+0.06}_{-0.03}$	4.2	CPP-MR	[73]
	0.76	0.43	0	Ab initio	[52]
	0.50 ± 0.03	0.45 ± 0.03	300	This paper	

C. Cu|FM interfaces

We proceed to study the SML at the interfaces between Cu and the FM metals Py and Co. The exchange interaction in FM metals automatically generates a spin polarization of the conduction electrons so we do not need to artificially inject a spin-polarized current from the half-metallic lead as in the previous section.

1. Cu|Py

Instead, we consider a Py thin film that is sandwiched between two diffusive Cu films, as sketched in Fig. 4(a). We pass an electric current through this multilayer and plot the calculated spin current as a function of position in Fig. 4(b). According to Eq. (5), it saturates to the value of the conductivity asymmetry β sufficiently deep into Py on a length scale of l_{Py}. The saturated plateau value decreases with increasing temperature corresponding to the suppression of β by magnons [50]. A lower but nonzero spin polarization is seen in the diffusive Cu layers. The spin current in Py and Cu can be fitted using Eqs. (5) and (6), respectively, as shown by the lines in Fig. 4. Unlike the corresponding Pt|FM|Pt case [51,56], the spin current does not show a significant discontinuity at the Py|Cu interface. A magnified plot about the right interface in Fig. 4(c) shows that a very small discontinuity appears only at low temperature. In particular, the quantitative calculation results in $\delta = 0$ at 300 K. After taking into account all the uncertainties in the calculated transport parameters entering Eqs. (9), we obtain an estimate of 0.09 as the upper limit of δ for the Cu|Py interface at room temperature. The interface spin asymmetry coefficient is estimated to be $\gamma = 0.97 \pm 0.01$, Table III. This high value can be understood in terms of the very similar majority-spin potentials of fcc Cu and of Fe and Ni in fcc Py [70], where the majority-spin $3d$ bands are calculated to be filled. The Cu|Py interface then scatters majority-spin electrons only very weakly. In contrast, the minority-spin potentials (and electronic structures) change abruptly at the interface, resulting in strong scattering. A highly asymmetric interface conductance is the result.

The very long SDL of Cu introduces two technical difficulties in the above calculations: (i) the value of l_{Cu} we use is extrapolated from high temperatures and (ii) the diffusive Cu layers attached to Py are not thick enough for the boundary condition $j_s(\pm\infty) = 0$ to be satisfied as required by the formulation of Sec. II C.

We first examine the robustness of our computational framework with respect to the value of l_{Cu}. In addition to using the value of $l_{\mathrm{sf}} \sim 502$ nm estimated by extrapolation in Fig. 1, we also use literature values of l_{Cu}, found in room-temperature experiments and listed in Table III to calculate δ and γ for the Cu|Py interface. Using these values in Eqs. (9) always yields a vanishingly small SML at room temperature. This is

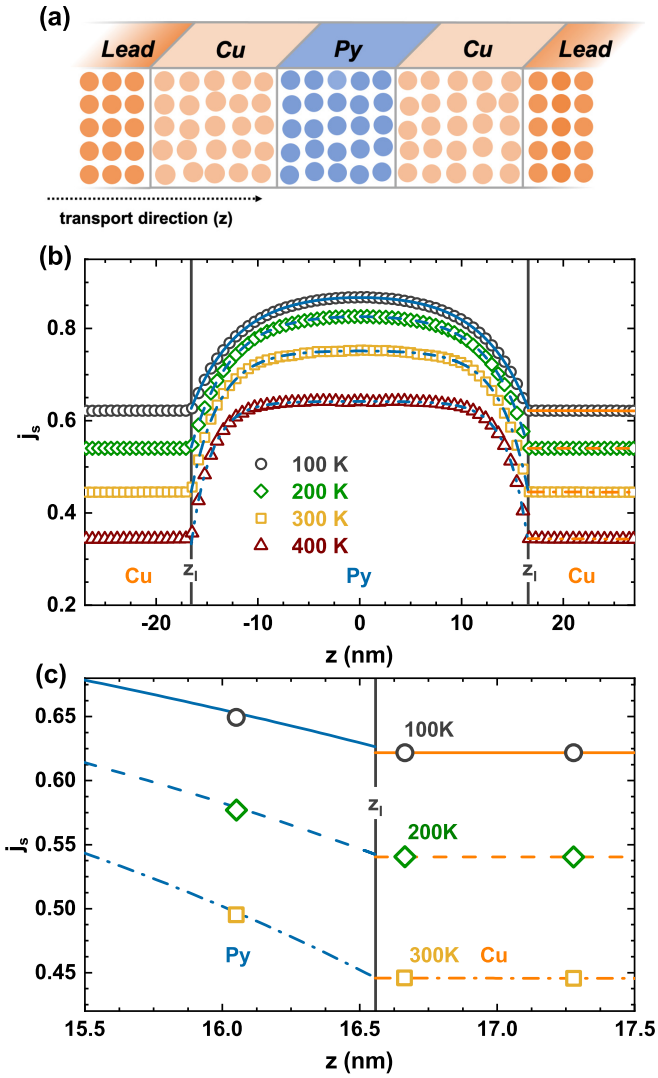

FIG. 4. (a) Schematic illustration of the scattering configuration for a thermally disordered Cu|Py|Cu trilayer sandwiched between ideal Cu leads. (b) Calculated spin current $j_s(z)$ in a Cu|Py|Cu multilayer at 100 K (circles), 200 K (diamonds), 300 K (squares), and 400 K (triangles). The solid, long-dashed, dash-dotted, and dotted curves are fits to Eq. (5) in Py (blue) and Eq. (6) in Cu (orange) at 100, 200, 300, and 400 K, respectively. (c) Magnified plot of the right Py|Cu interface.

insensitive to the particular value of l_{Cu} used and only its upper bound shows a slight variation. The value of γ we estimate is relatively sensitive to the value of l_{Cu} used; a longer l_{Cu} results

TABLE III. Comparison of the values of l_{Cu} (nm), $\rho_{\mathrm{Cu}}l_{\mathrm{Cu}}$ (fΩ m^2), γ, and δ we calculate for the Cu|Py (111) interface at room temperature, this paper, with values of $\delta_{\mathrm{Cu|Py}}$ and $\gamma_{\mathrm{Cu|Py}}$ we estimate using values of l_{Cu} and $\rho_{\mathrm{Cu}}l_{\mathrm{Cu}}$ reported from various experiments. LNL/M: Lateral nonlocal MR with metallic contacts and no other special conditions. LNL/+: Lateral nonlocal MR with an extra strip or strips across the NM-metal. LNL/C: Lateral nonlocal MR using a cross geometry for the NM metal. CPP-NP: CPP-MR using electron-beam lithography produced nanopillar trilayers. CPP-NW: CPP-MR using electrodeposited nanowire multilayers. The value of l_{Cu} that we extrapolate from the first-principles calculations at high temperatures shown in Fig. 1 is also listed for comparison.

T(K)	Method	l_{Cu}(nm)	$\rho_{\mathrm{Cu}}l_{\mathrm{Cu}}$	$\delta_{\mathrm{Cu|Py}}$	$\gamma_{\mathrm{Cu|Py}}$
300	CPP-NW [97]	36 ± 14	0.4–3	$0^{+0.07}$	0.42 ± 0.35
300	LNL/M [98]	110	4	$0^{+0.09}$	0.85 ± 0.03
293	CPP − NP [99]	170 ± 40		$0^{+0.08}$	0.91 ± 0.06
293	LNL/C [64,100]	350 ± 50	10	$0^{+0.09}$	0.96 ± 0.02
293	LNL/M; LNL/+ [101]	500	11	$0^{+0.09}$	0.97 ± 0.01
293	LNL/M [102]	700	15	$0^{+0.09}$	0.98 ± 0.01
300	This paper	502	9.0 ± 1.0	$0^{+0.09}$	0.97 ± 0.01

in a larger value of γ. This is because the normalized spin currents $j_s(z_{\mathrm{I}}+\eta)$ on the Cu side and $j_s(z_{\mathrm{I}}-\eta)$ on the Py side of the interface have values between 0 and 1 and the large product $\rho_{\mathrm{Cu}}l_{\mathrm{Cu}}$ in Eqs. (9) must be compensated by the factor $1-\gamma^2$ to avoid exceeding these bounds. In particular, we see that in the limit $l_{\mathrm{Cu}} \to \infty$, $\gamma = 1$. Therefore, a reasonable value of l_{Cu} is needed to estimate γ, the interface resistance asymmetry.

The large value of $l_{\mathrm{Cu}} \sim 502$ nm makes it impossible to construct a scattering region long enough for a Cu|FM|Cu trilayer to satisfy the boundary condition $j(\pm\infty) = 0$ in currently practical calculations. We therefore examine the values of δ and γ we obtain when we apply a different boundary condition that can be strictly complied with in practice. By analogy with the injection of a fully polarized current into the Cu|Pt bilayer, we can inject a fully spin-polarized current with the same polarization sign as Py into a Cu|Py bilayer; this then satisfies the condition $j_s(-\infty) = 1$. When the thickness of Py is much larger than its SDL, the spin current approaches its bulk polarization β at $z \to +\infty$. Following the same procedure we used for the NM|NM′ interface in Sec. II B, we derive the semiclassical diffusion equations for spin transport in a diffusive NM|FM bilayer in the Appendix to eventually arrive at the two equations

$$j_s(z_{\mathrm{I}}-\eta) = \gamma - \frac{(1-\gamma^2)\delta}{AR_{\mathrm{I}}\sinh\delta}\left\{\frac{\rho_{\mathrm{FM}}l_{\mathrm{FM}}}{1-\beta^2}[j_s(z_{\mathrm{I}}+\eta)-\beta] - \rho_{\mathrm{NM}}l_{\mathrm{NM}}\left[\mathrm{csch}\left(\frac{z_{\mathrm{I}}}{l_{\mathrm{NM}}}\right) - j_s(z_{\mathrm{I}}-\eta)\coth\left(\frac{z_{\mathrm{I}}}{l_{\mathrm{NM}}}\right)\right]\cosh\delta\right\}, \quad (11a)$$

$$j_s(z_{\mathrm{I}}+\eta) = \gamma - \frac{(1-\gamma^2)\delta}{AR_{\mathrm{I}}\sinh\delta}\left\{\frac{\rho_{\mathrm{FM}}l_{\mathrm{FM}}}{1-\beta^2}[j_s(z_{\mathrm{I}}+\eta)-\beta]\cosh\delta - \rho_{\mathrm{NM}}l_{\mathrm{NM}}\left[\mathrm{csch}\left(\frac{z_{\mathrm{I}}}{l_{\mathrm{NM}}}\right) - j_s(z_{\mathrm{I}}-\eta)\coth\left(\frac{z_{\mathrm{I}}}{l_{\mathrm{NM}}}\right)\right]\right\}. \quad (11b)$$

The spin current $j_s(z)$ calculated in the Cu|Py bilayer with the boundary condition $j_s(-\infty) = 1$ is plotted in Fig. 5. Using Eq. (6) to fit the data calculated in Cu (solid orange line) and Eq. (5) for those in Py (solid blue line) allows us to find the asymptotic values $j_s(z_{\mathrm{I}} \pm \eta) = 0.998$ at the interface. Since all the bulk parameters ρ_{NM}, l_{NM}, ρ_{FM}, l_{FM}, and β as well as

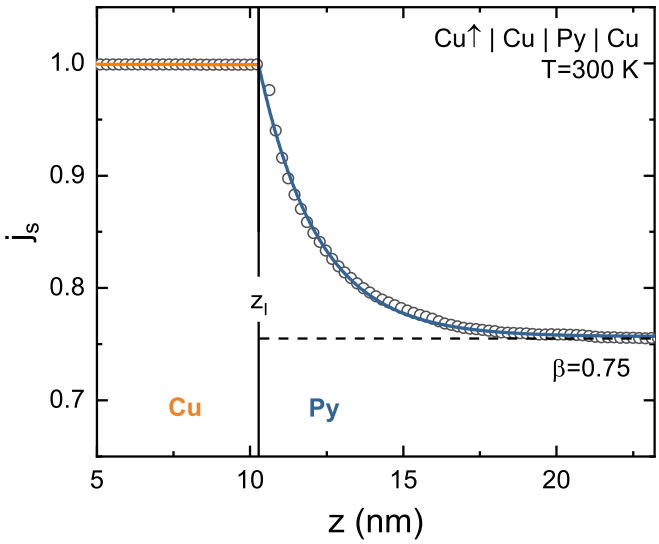

FIG. 5. Spin current $j_s(z)$ calculated for a Cu|Py bilayer when a fully spin-polarized current is injected into Cu from the left electrode (empty circles) corresponding to the boundary condition $j_s(-\infty) = 1$. The polarization decays in the Cu|Py bilayer and approaches the bulk spin polarization well inside Py, resulting in $j_s(+\infty) = \beta$. Here the bulk value $\beta = 0.75$ is illustrated by the dashed line. The solid lines are fits with Eq. (5) to determine $j_s(z_I \pm \eta)$, which are used to solve δ and γ in Eq. (11).

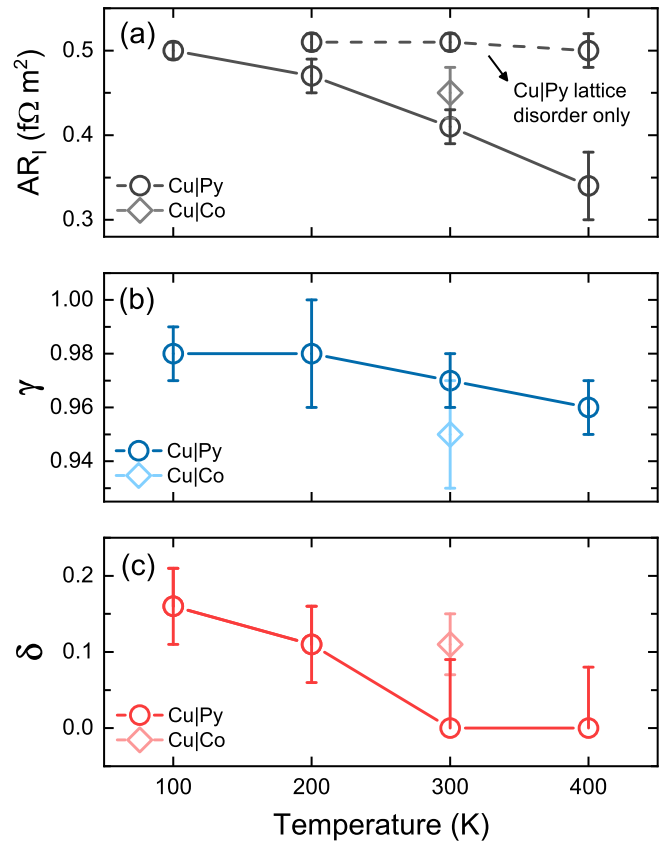

FIG. 6. Interface parameters AR_I (a), γ (b), and δ (c) for Cu|Py interface (circles) extracted from the spin currents as a function of temperature. The black circles with a dashed line in (a) show the calculated AR_I for the Cu|Py interface with only lattice disorder. The corresponding parameters for Cu|Co interface at room temperature are also shown (diamonds) for comparison.

the interface resistance AR_I were already determined independently, Eq. (11) can be solved resulting in $\delta = 0^{+0.05}$ and $\gamma = 0.99 \pm 0.01$. Here the uncertainties in δ and γ are obtained by considering the uncertainties in all the other parameters in Eq. (11). This independent check with an alternative boundary condition confirms the values $\delta = 0^{+0.09}$ and $\gamma = 0.97 \pm 0.01$ extracted from Fig. 4 using the trilayer structures. It is worth noting that the thickness of Py in the Cu|Py bilayer must be large enough to satisfy the boundary condition $j_s(+\infty) = \beta$. Otherwise the Cu right-hand lead may influence the values of j_s calculated near the Cu|Py interface. (Indeed, the influence of the right-hand lead can be seen in the incipient deviation of $j_s(z)$ from β for $z > 20$ nm in Fig. 5.)

The temperature dependence of AR_I, δ and γ is shown in Fig. 6 for the Cu|Py interface. All three parameters decrease monotonically with increasing temperature and this decrease can be attributed to the stronger spin disorder of Py at higher temperature by analogy with our findings for the Pt|Py interface [51]. The electron scattering at the Cu|Py interface is strongly spin dependent: the majority-spin channel is highly conductive and, without spin-orbit coupling or spin disorder, the minority-spin channel is much more resistive. Spin disorder allows the spins of conduction electrons to flip at the interface and hence reduces the transmission of majority-spin electrons. At the same time, it creates more transmission channels for minority-spin electrons. Because the minority-spin 3d bands are partially occupied for Py, their state density at the Fermi energy is very large so the increase of the minority-spin conductance is greater than the decrease of that for the majority spins. Therefore, the total transmission probability increases with increasing spin disorder; the interface resistance decreases. To confirm this, we repeat the $T = 200$ K, 300 K, and 400 K calculations for the Cu|Py interface with only lattice disorder and keep the magnetic moments aligned with the global quantization axis. The values of AR_I we calculate are almost independent of temperature, as shown in Fig. 6. We conclude that spin disorder is the main reason for the temperature-induced decrease of the interface resistance.

The Cu|Py interface parameters we calculate at various temperatures are listed in Table IV. The low temperature ($T = 100$ K) value of $AR_I = 0.5\,\text{f}\Omega\,\text{m}^2$ that we calculate is in reasonable agreement with the low-temperature experimental value of 0.26 fΩ m^2 [103]. The discrepancy may be

TABLE IV. Interface parameters AR_I, γ and δ extracted from the currents calculated for Cu|Py and Cu|Co interfaces from first-principles at various temperatures.

	T(K)	AR_I(fΩ m^2)	γ	δ
Cu|Py	100	0.50 ± 0.01	0.98 ± 0.01	0.16 ± 0.05
	200	0.47 ± 0.02	0.98 ± 0.02	0.11 ± 0.05
	300	0.41 ± 0.02	0.97 ± 0.01	$0^{+0.09}$
	400	0.34 ± 0.04	0.96 ± 0.01	$0^{+0.08}$
Cu|Co	300	0.45 ± 0.03	0.95 ± 0.02	0.11 ± 0.04

attributed to unknown microscopic interface disorder in the experimental samples. Accurate measurements of the interface resistance depend on being able to separate bulk and interface contributions clearly but these are usually strongly entangled [73]. The calculated value of $\gamma = 0.97 \pm 0.01$ is also larger than the experimental value 0.7 [103]. Improved characterization of the experimental interface structures are necessary to make progress. The SML δ is approximately 0.16 ± 0.05 at 100 K and becomes negligible at room temperature, indicating that the Cu|Py interface is transparent to a spin current. As the interfacial counterpart of bulk SDL, the SML arises microscopically from the spin-flip scattering at the interface, which is usually induced by the enhanced spin-orbit interaction owing to the broken translational symmetry. With increasing temperature, spin fluctuation in the FM provides an additional source of spin-flip scattering. Nevertheless, the temperature-induced spin fluctuation also lowers the spin-polarization parameter β in bulk [51,56]. Overall, the calculated SML for Cu|Py exhibits a monotonic decrease with increasing temperature.

2. Cu|Co

We repeat the above calculations at room temperature replacing Py by Co, which has a higher Curie temperature and no intrinsic alloy disorder. The calculated interface parameters are included in Fig. 6. A value of $AR_{\mathrm{Cu|Co}} = 0.45 \pm 0.03\,\mathrm{f\Omega\,m^2}$ is found which can be compared with the low-temperature experimental value of $0.20\,\mathrm{f\Omega\,m^2}$ [103] and previously calculated value of $0.31\,\mathrm{f\Omega\,m^2}$ without spin-orbit coupling and thermal disorder [46]. We find a value of $\gamma = 0.95 \pm 0.02$ that is larger than the experimental value of $\gamma = 0.77 \pm 0.04$ [103]. The room temperature SML, $\delta = 0.11 \pm 0.04$, for the Cu|Co interface compares reasonably with the low-temperature experimental value $\delta = 0.33^{+0.03}_{-0.08}$ [103]. The values of AR_{I} and δ we calculate for the Cu|Co interface are slightly larger than the corresponding values for the Cu|Py interface because of the greater order of Co. We found analogous results for Pt|Py and Pt|Co interfaces [51]. $\gamma_{\mathrm{Cu|Co}}$ is nearly the same as $\gamma_{\mathrm{Cu|Py}}$, indicating the strong spin-filtering effect of both interfaces.

D. Interface mixing

Even in the best experimental samples, the interfaces will almost certainly not be as well ordered as those we have considered so far. In the process of growing thin layers, the kinetic energy of the deposited atoms will lead to interface mixing, rendering the interfaces less sharp [73]. We model the mixing of an A|B interface by completely mixing one (or two) layers on either side of the interface that then leads to two (or four) layers with the composition $\mathrm{A_{50}B_{50}}$. The lattice and spin disorder is assumed to be unchanged, as are the atomic sphere potentials. The spin currents that result from these calculations for Cu|Py|Cu structures with intermixed interfaces are shown in Fig. 7(a). They are fitted in Py and Cu using Eqs. (5) and (6), respectively, and extrapolated to the Py|Cu interface at z_{I} to determine $j_s(z_{\mathrm{I}} - \eta)$ on the Py side and $j_s(z_{\mathrm{I}} + \eta)$ on the Cu side, Fig. 7(a), lower panel. The interface resistance AR_{I} is determined in separate calculations and, finally, δ and γ are extracted by solving Eq. (9). The results are shown for both Cu|Py and Cu|Co interfaces in Fig. 7(b). AR_{I} is seen to increase monotonically with increasing thickness of the mixed interface layer because of the strong scattering by alloy disorder. The interface spin asymmetry parameter γ is not changed by the intermixing. The majority-spin potentials of Co, and of both Ni and Fe in Py, are perfectly matched to the potential of Cu while the minority-spin potentials all differ. For this reason, both Cu|Py and Cu|Co interfaces exhibit strong spin filtering and this effect is not significantly weakened by mixing the magnetic and Cu atoms.

The effect of interface mixing on the SML for Cu|Py and Cu|Co interfaces is complex. First, the stronger interface scattering by the interface alloy enhances the spin flipping, as we found for the NM Au|Pt interface [51]. For a Cu|FM interface, alloying reduces the magnetic order on the FM side and this reduces the SML by analogy with the reduction we found for Pt|Co and Pt|Py interfaces on increasing the temperature [51]. Competition between the two effects results in the (slightly) nonmonotonic dependence of δ on the thickness of the interface alloy layer at Cu|Py and Cu|Co interfaces shown in Fig. 7(b). This nonmonotonic behavior is clearer for Cu|Co since Co has a higher degree of magnetic order than Py.

E. Inserting copper at a FM|NM interface

Cu is commonly used in experiments as a spacer material between a heavy metal like Pt with a large spin susceptibility and a FM metal to prevent magnetism being induced in Pt by the proximity effect. Because of its weak spin-orbit interaction and correspondingly long SDL, a thin layer of Cu is usually assumed to have no effect on a spin current, thus making the interpretation of experiments simpler. However, though bulk Cu may have little effect on a spin current, insertion of a Cu layer between a FM metal and Pt replaces the single FM|Pt interface with two different interfaces, namely, FM|Cu and Cu|Pt interfaces whose effect on a spin current is, at best, poorly known. Here we consider Py and Co as typical FM metals and Pt as a typical heavy metal to investigate the influence of inserting Cu layers on the SML.

As shown schematically in Fig. 8(a), we calculate the spin current distribution at 300 K for a Pt|Cu|Py|Cu|Pt multilayer when a charge current is passed through it. The thickness of the Py (Pt) layers is 26 nm (25 nm) and we consider $N = 0$, 1, and 2 atomic layers of Cu. The spin current in the transport direction (z) that we calculate for a symmetric Pt|Cu(N)|Py|Cu(N)|Pt multilayer is shown in Fig. 8(b) for $N = 2$. Both the saturated plateau in the center of Py and the vanishing spin current at the interfaces between Pt and the leads confirm that Py and Pt are sufficiently thick and satisfy the boundary condition $j_s(\pm\infty) = 0$. We fit $j_s(z)$ using the spin diffusion equations in Py and Pt and use these fits to extrapolate $j_s(z)$ on the Py side to the Py|Cu interface to calculate $j_s(z_{\mathrm{I}} - \eta)$ and on the Pt side to the Cu|Pt interfaces to calculate $j_s(z_{\mathrm{I}} + \eta)$, respectively as illustrated in the exploded plot in Fig. 8(c). The somewhat arbitrary choice of z_{I} within the Cu insert has a negligible effect

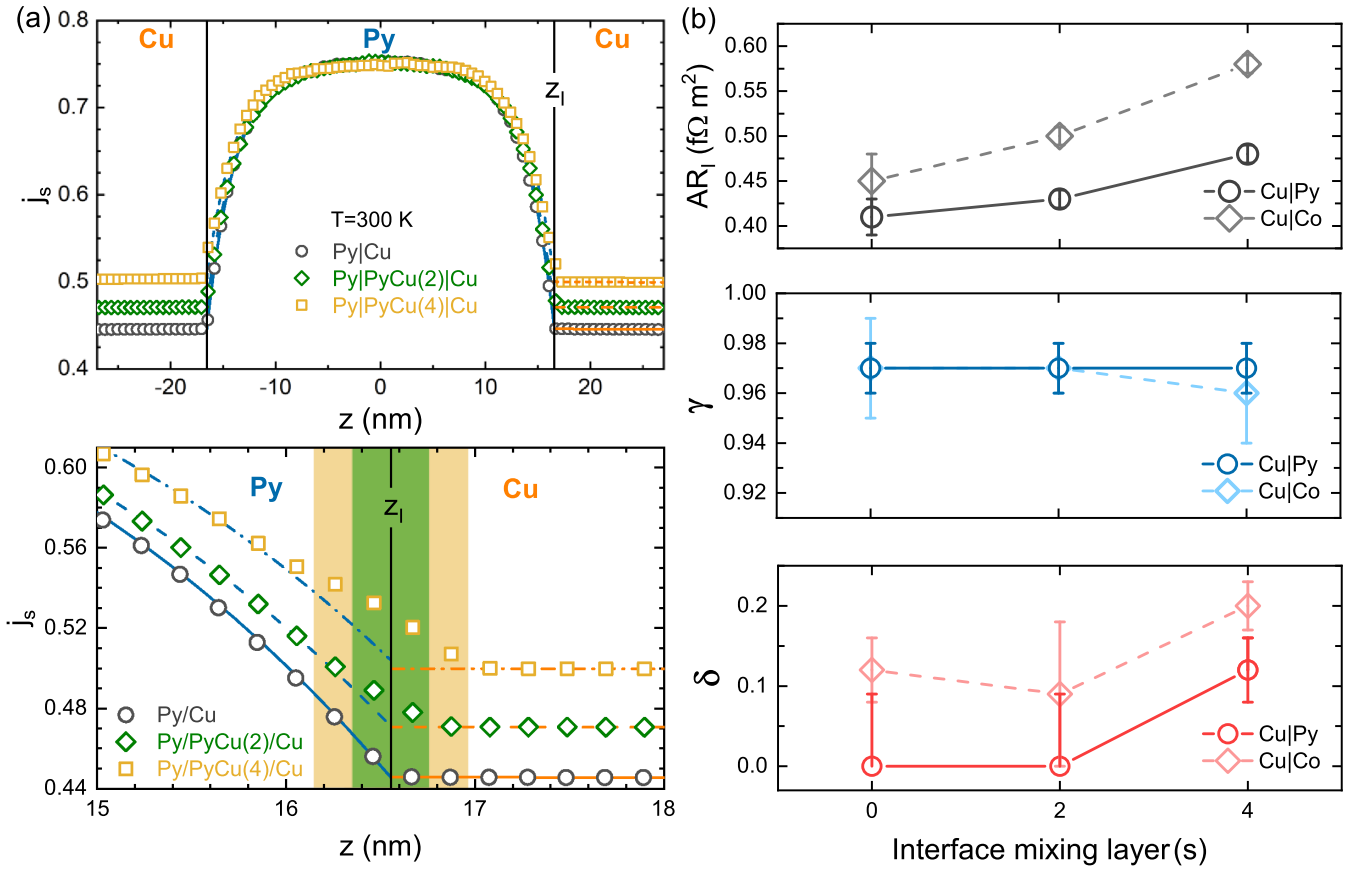

FIG. 7. (a) Spin currents $j_s(z)$ calculated for sharp (grey circles) and mixed Cu|Py interfaces with two (green diamonds) and four (yellow squares) atomic layers of mixed interface modeled as $Py_{50}Cu_{50}$ alloy. Thermal lattice and spin disorder are chosen to reproduce experimental room-temperature bulk resistivities. The lower panel shows an exploded view of the right Py|Cu interface. The solid, dashed, and dash-dotted curves are fits to Eqs. (5) in Py (blue) and (6) in Cu (orange) for the sharp interface (vertical line at z_I), two (vertical green shading) and four (vertical yellow shading) mixed interface layers, respectively. (b) Interface parameters AR_I (grey), γ (blue), and δ (red) with $N = 0, 2, 4$ mixed interface layers for Cu|Py (circles, solid lines) and Cu|Co (diamonds, dashed lines) interfaces.

on the values of δ and γ that we extract because of the thinness of Cu. The SML determined in this way accounts for the spin-flipping at the compound interface between Py and Pt.

Using the above scheme, we calculate the interface parameters AR_I, γ and δ for Py|Cu|Pt and Co|Cu|Pt interfaces at room temperature and summarize the results in Fig. 9 and Table V. The Cu insert increases $AR_{Py|Pt}$ to between 1.06 and 1.11 fΩ m^2, which is very close to the sum of the two interface resistances connected in series, $AR_{Py|Cu} + AR_{Cu|Pt} = 1.05 \pm 0.04$ fΩ m^2. Because Cu is so thin and conductive, its contribution to AR_I can be neglected. The parameter γ is small for both the Py|Pt and Co|Pt interfaces but increases with increasing Cu thickness. This is because the Py|Cu and Co|Cu interfaces have strong spin filtering effects. The scattering rate for minority-spin electrons is enhanced by the Cu insert leading to an increase in γ. The dependence of AR_I and γ on the thickness of Cu is the same for both Py|Cu|Pt and Co|Cu|Pt interfaces.

TABLE V. Calculated interface parameters AR_I, γ, and δ for N atomic layers of Cu ($N = 0, 1, 2$) inserted into the Py|Pt and Co|Pt interfaces at room temperature.

	N	AR_I(fΩ m^2)	γ	δ
Py|Cu(N)|Pt	0	0.79 ± 0.03	-0.06 ± 0.09	0.76 ± 0.11
	1	1.06 ± 0.02	0.09 ± 0.09	0.86 ± 0.12
	2	1.11 ± 0.01	0.14 ± 0.07	1.00 ± 0.14
Co|Cu(N)|Pt	0	0.82 ± 0.05	0.00 ± 0.08	0.77 ± 0.13
	1	1.11 ± 0.01	0.12 ± 0.03	1.12 ± 0.16
	2	1.12 ± 0.01	0.17 ± 0.05	1.18 ± 0.17

We finally consider the SML with and without the Cu insert. Without it, $\delta_{Py|Pt} = 0.76 \pm 0.11$ at room temperature. As shown in Table V and Fig. 9, inserting Cu increases $\delta_{Py|Pt}$ slightly to 0.86 ± 0.12 for $N = 1$ and to 1.00 ± 0.14 for $N = 2$ compared to $\delta_{Py|Cu} + \delta_{Cu|Pt} = (0.00^{+0.09}) + (0.77 \pm 0.04) = 0.77 \pm 0.10$ for the two separate interfaces. For the Co|Pt interface, the SML increases from $\delta_{Co|Pt} = 0.77 \pm 0.13$ to 1.12 ± 0.16 for $N = 1$ and 1.18 ± 0.17 for $N = 2$. The sum of the room-temperature SML values for the individual interfaces, $\delta_{Co|Cu} + \delta_{Cu|Pt} = (0.11 \pm 0.04) + (0.77 \pm 0.04) = 0.88 \pm 0.06$, is substantially lower than the SML we find for the compound Co|Cu|Pt interface. Thus, contrary to the expectation that separating the FM and heavy metal should enhance the interface transparency for a spin current [104], we find that it increases the SML.

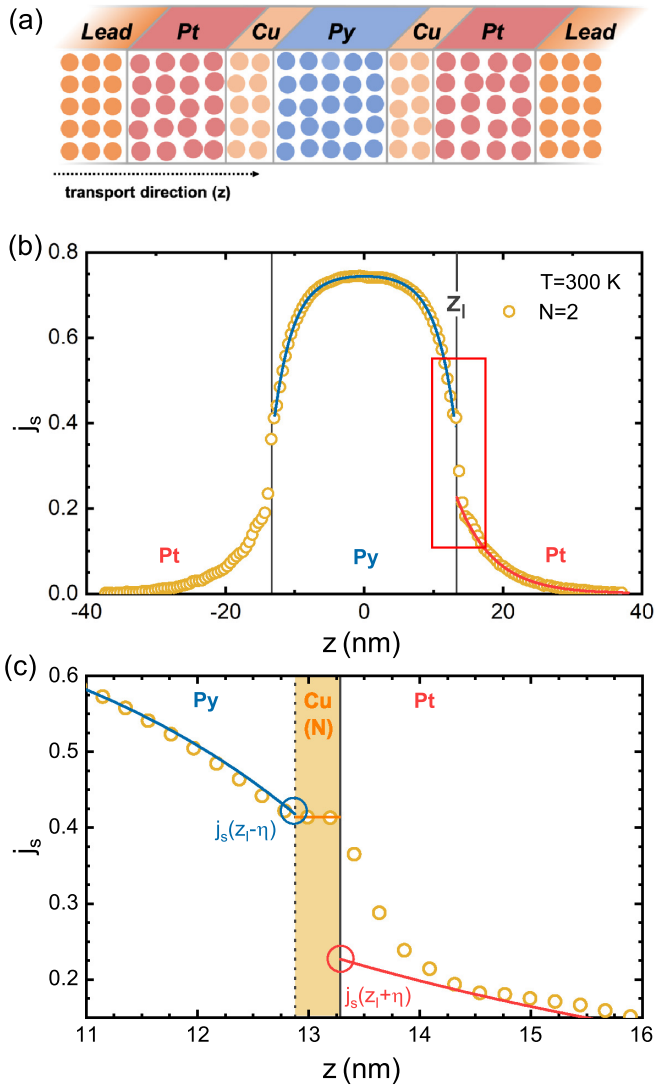

FIG. 8. (a) Sketch of a Pt|Cu|Py|Cu|Pt multilayer sandwiched between semi-infinite ballistic Cu leads. All atoms in the scattering region are displaced from their equilibrium positions on fcc lattices to simulate room-temperature lattice disorder. Spin disorder in Py is included in the same way as before. (b) Spin current $j_s(z)$ calculated for a Pt|Cu(2)|Py|Cu(2)|Pt multilayer where two atomic layers of Cu are inserted at the Py|Pt interfaces. An exploded view of the discontinuity inside the red rectangle about the right-hand Py|Cu|Pt interface is shown in (c) where the solid lines represent the piecewise fitting in Py and Pt using the solution to the spin diffusion Eqs. (5) and (6), respectively. These fits are extrapolated to a position z_I between the Py|Cu and Cu|Pt interface to obtain the values $j_s(z_I - \eta)$ and $j_s(z_I + \eta)$, respectively, indicated schematically by the large open circles. Shifting the position z_I about inside Cu has a negligible effect on the values of γ and δ we extract because of the thinness of Cu. The Cu insert is considered as a compound Py|Pt interface.

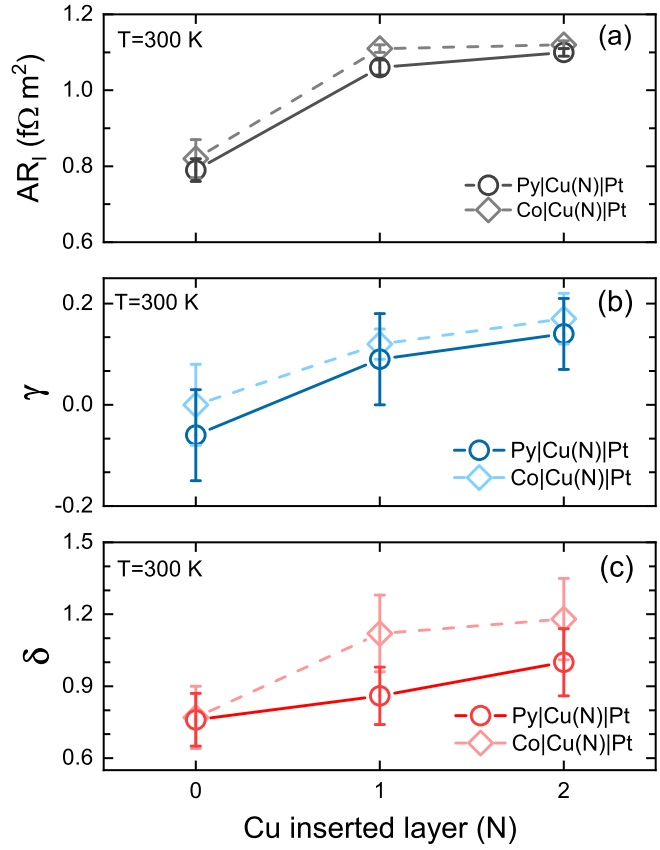

FIG. 9. Calculated interface resistance AR_I (a), spin-asymmetry parameter γ (b), and SML δ (c) when N atomic layers of Cu ($N = 0, 1, 2$) are inserted into the Py|Pt (circles) and Co|Pt (diamonds) interfaces at room temperature. The solid and dashed lines are guides to the eye.

IV. CONCLUSION

We have calculated the semiclassical spin transport parameters for Cu|Pt, Cu|Pd, Cu|Py, and Cu|Co interfaces at finite temperature within the adiabatic approximation using first-principles scattering theory [70] and a recently developed planar-averaged local current scheme [42]. The dependence of the interface parameters on temperature and interface atomic mixing is studied systematically. The SML at a Cu|Pt interface is comparable to what we found for an incommensurate Au|Pt interface in Ref. [51], which we attribute to the similarity of the free-electron-like electronic structures of the noble metals Cu and Au. For Cu|Py and Cu|Co interfaces, both the interface resistance and SML are found to decrease monotonically with temperature. The SML becomes negligibly small at room temperature. By analogy with the Pt|FM interfaces, the SML is larger for Cu|Co than for Cu|Py because unlike Py, Co does not have alloy disorder and has a higher Curie temperature. Inserting a thin layer of Cu in the Py|Pt or Co|Pt interfaces increases the SML. Since Cu is widely used as a transport channel in nonlocal spin valves, our calculated values of interface transport parameters for the Cu|NM and Cu|FM interfaces should be very useful reference data for experimental studies.

Where comparison can be made, the results we calculate are in reasonable agreement with published experimental values. The sophistication of our calculations is such that where discrepancies exist, the first issue that must be examined is the validity of the structural models we use. Our computer codes make it possible to examine many types of interface disorder but at present more information is required from experiment to motivate more extensive theoretical investigations than the

present one. Where the experimental data were obtained from low-temperature models, the onus is on our experimental colleagues to provide us with information about the disorder that leads to diffusive behavior at low temperatures.

ACKNOWLEDGMENTS

This work was financially supported by the National Natural Science Foundation of China (Grants No. 12174028 and No. 11734004), the Recruitment Program of Global Youth Experts, and by the Nederlandse Organisatie voor Wetenschappelijk Onderzoek (NWO) through the research program of the former Stichting voor Fundamenteel Onderzoek der Materie, (NWO-I, formerly FOM). K.G. acknowledges funding from the Shell-NWO/FOM Computational Sciences for Energy Research PhD program (CSER-PhD; nr. i32; Project number 13CSER059). The work was also supported by the Royal Netherlands Academy of Arts and Sciences (KNAW).

APPENDIX: THE VALET-FERT FORMALISM FOR A NM|FM BILAYER

The RT value of $l_{\rm Pt} \sim 5.3$ nm makes it possible to realize the boundary condition $j_s(\pm\infty) \to 0$ for Pt|FM|Pt scattering regions that can be handled in practical calculations [51,56]. The large value of $l_{\rm Cu} \sim 502$ nm makes this impossible for Cu|FM|Cu raising doubts about the value of δ calculated in Sec. III C. In this Appendix, we derive semiclassical transport equations based on the Valet-Fert formalism for a NM|FM bilayer with a spin-polarized current incident from the left lead for which the boundary condition is $j_s(-\infty) = \pm 1$. Using this alternative boundary condition to determine the SML for Cu|FM interfaces yields the same numerical values of δ as the $j_s(\pm\infty) \to 0$ boundary condition. We demonstrate that the two different calculation schemes yield the same results within the numerical accuracy for a Pt|Py interface.

We follow the standard procedure used in the literature [30,32] and treat the interface (I) as an artificial bulklike material with resistivity $\rho_{\rm I}$, SDL $l_{\rm I}$ and finite thickness t that are related to an interface resistance and SML as $AR_{\rm I} = \rho_{\rm I} t$ and $\delta = t/l_{\rm I}$. The general solutions (3) and (5) to the spin diffusion equations and Ohm's law have the same forms in the NM, I (interface), and FM regions:

$$\mu_{si}(z) = A_i e^{z/l_i} + B_i e^{-z/l_i}, \tag{A1}$$

$$j_{si}(z) = \beta_i - \frac{1-\beta_i^2}{2ej\rho_i l_i}\left(A_i e^{z/l_i} - B_i e^{-z/l_i}\right). \tag{A2}$$

If a fully polarized spin current is injected from an artificial half-metallic left lead into a diffusive NM|FM bilayer, one has the boundary condition $j_{s,\rm NM}(0) = \pm 1$, where the sign $+(-)$ indicates that the polarization is parallel (antiparallel) to the current polarization direction in the FM metal. Substituting this boundary condition at $z = 0$ into Eq. (A2) and considering $\beta = 0$ in the NM metal, we find

$$A_{\rm NM} = B_{\rm NM} \mp 2ej\rho_{\rm NM} l_{\rm NM}. \tag{A3}$$

The above equation can be substituted into Eqs. (A1) and (A2) to eliminate the coefficients $A_{\rm NM}$ and $B_{\rm NM}$. Eventually, we arrive at the following relation between the spin accumulation $\mu_{s,\rm NM}$ and the normalized spin current $j_{s,\rm NM}$ in the NM metal:

$$\mu_{s,\rm NM} = \frac{2ej\rho_{\rm NM} l_{\rm NM}}{\sinh(z/l_{\rm NM})}\left[\pm 1 - j_{s,\rm NM}(z)\cosh(z/l_{\rm NM})\right]. \tag{A4}$$

In the FM metal, the boundary condition $j_{s,\rm FM}(+\infty) = \beta$ results in $A_{\rm FM} = 0$. The other coefficient $B_{\rm FM}$ can be eliminated using Eqs. (A1) and (A2) and the spin accumulation in the FM metal reads

$$\mu_{s,\rm FM}(z) = \frac{2ej\rho_{\rm FM} l_{\rm FM}}{1-\beta^2}\left[j_{s,\rm FM}(z) - \beta\right]. \tag{A5}$$

Since the interface is replaced by an artificial bulklike material with a finite thickness t, the spin accumulation $\mu_s(z)$ and spin current $j_s(z)$ are continuous everywhere. At the NM|I boundary $z = z_{\rm I}$ and at the I|FM boundary $z = z_{\rm I} + t$, the spin accumulation μ_s and spin current j_s are both continuous:

$$\mu_{s,\rm NM}(z_{\rm I}) = \mu_{s,\rm I}(z_{\rm I}) = A_{\rm I} e^{z_{\rm I}/l_{\rm I}} + B_{\rm I} e^{-z_{\rm I}/l_{\rm I}}, \tag{A6}$$

$$\mu_{s,\rm FM}(z_{\rm I}+t) = \mu_{s,\rm I}(z_{\rm I}+t) = A_{\rm I} e^{(z_{\rm I}+t)/l_{\rm I}} + B_{\rm I} e^{-(z_{\rm I}+t)/l_{\rm I}}, \tag{A7}$$

$$j_{s,\rm NM}(z_{\rm I}) = j_{s,\rm I}(z_{\rm I}) = \gamma - \frac{1-\gamma^2}{2ej\rho_I l_{\rm I}}(A_{\rm I} e^{z_{\rm I}/l_{\rm I}} - B_{\rm I} e^{-z_{\rm I}/l_{\rm I}}), \tag{A8}$$

$$j_{s,\rm FM}(z_{\rm I}+t) = j_{s,\rm I}(z_{\rm I}+t) = \gamma - \frac{1-\gamma^2}{2ej\rho_I l_{\rm I}} \times (A_{\rm I} e^{(z_{\rm I}+t)/l_{\rm I}} - B_{\rm I} e^{-(z_{\rm I}+t)/l_{\rm I}}). \tag{A9}$$

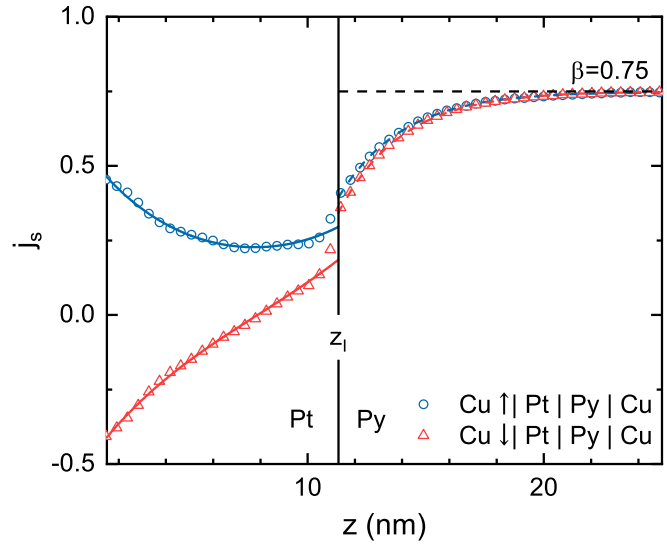

FIG. 10. Spin currents $j_s(z)$ calculated inside a diffusive Pt(10 nm)|Py(15 nm) bilayer at room temperature. Fully polarized spin-up (blue circles) and spin-down (red triangles) currents injected from artificial half-metallic Cu(↑) and Cu(↓) left leads, respectively. The magnetization of Py is set as its polarization $\beta > 0$ indicated by the horizontal dashed line. Each data is an average over 20 random configurations of thermal lattice and spin disorder. The solid and dashed lines are fits using (A2) in Pt and Py, respectively, with appropriate boundary conditions.

Equations (A6) and (A7) can be used to express the coefficients $A_{\rm I}$ and $B_{\rm I}$ as functions of the spin accumulation at the NM|I and I|FM boundaries as

$$A_{\rm I} = \frac{\mu_{s,{\rm NM}}(z_{\rm I})e^{-t/l_{\rm I}} - \mu_{s,{\rm FM}}(z_{\rm I}+t)}{e^{z_{\rm I}/l_{\rm I}}(e^{-t/l_{\rm I}} - e^{t/l_{\rm I}})}, \tag{A10}$$

$$B_{\rm I} = \frac{\mu_{s,{\rm NM}}(z_{\rm I})e^{t/l_{\rm I}} - \mu_{s,{\rm FM}}(z_{\rm I}+t)}{e^{-z_{\rm I}/l_{\rm I}}(e^{t/l_{\rm I}} - e^{-t/l_{\rm I}})}. \tag{A11}$$

Substituting Eqs. (A10) and (A11) into Eqs. (A8) and (A9), we find two equations containing μ_s and j_s at the boundaries $z = z_{\rm I}$ and $z = z_{\rm I} + t$. The spin accumulation μ_s is eliminated using Eqs. (A4) and (A5) and, finally, we take the limit $t \to 0$ to arrive at Eq. (11) that only depend on spin currents

$$j_{s,{\rm NM}}(z_{\rm I}) = \gamma - \frac{(1-\gamma^2)\delta}{AR_{\rm I}\sinh\delta}\left\{\frac{\rho_{\rm FM}l_{\rm FM}}{1-\beta^2}[j_{s,{\rm FM}}(z_{\rm I}) - \beta] - \rho_{\rm NM}l_{\rm NM}\left[\pm{\rm csch}\left(\frac{z_{\rm I}}{l_{\rm NM}}\right) - j_{s,{\rm NM}}(z_{\rm I}){\rm coth}\left(\frac{z_{\rm I}}{l_{\rm NM}}\right)\right]\cosh\delta\right\}, \tag{A12a}$$

$$j_{s,{\rm FM}}(z_{\rm I}) = \gamma - \frac{(1-\gamma^2)\delta}{AR_{\rm I}\sinh\delta}\left\{\frac{\rho_{\rm FM}l_{\rm FM}}{1-\beta^2}[j_{s,{\rm FM}}(z_{\rm I}) - \beta]\cosh\delta - \rho_{\rm NM}l_{\rm NM}\left[\pm{\rm csch}\left(\frac{z_{\rm I}}{l_{\rm NM}}\right) - j_{s,{\rm NM}}(z_{\rm I}){\rm coth}\left(\frac{z_{\rm I}}{l_{\rm NM}}\right)\right]\right\}. \tag{A12b}$$

Here $j_{s,{\rm NM}}(z_{\rm I}) \equiv j_s(z_{\rm I} - \eta)$ in Eq. (11) and similarly $j_{s,{\rm FM}}(z_{\rm I}) \equiv j_s(z_{\rm I} + \eta)$ and we have already made use of the relations $\rho_{\rm I}t = AR_{\rm I}$ and $t/l_{\rm I} = \delta$.

For the special case $\beta = \gamma = 0$, the NM|FM interface becomes an NM|NM′ interface and Eqs. (A12a) and (A12b) reduce to

$$j_{s,{\rm NM}}(z_{\rm I}) = \frac{\delta}{AR_{\rm I}\sinh\delta}\left\{-\rho_{\rm NM'}l_{\rm NM'}j_{s,{\rm NM'}}(z_{\rm I}) + \rho_{\rm NM}l_{\rm NM}\left[\pm{\rm csch}\left(\frac{z_{\rm I}}{l_{\rm NM}}\right) - j_{s,{\rm NM}}(z_{\rm I}){\rm coth}\left(\frac{z_{\rm I}}{l_{\rm NM}}\right)\right]\cosh\delta\right\}, \tag{A13a}$$

$$j_{s,{\rm NM'}}(z_{\rm I}) = \frac{\delta}{AR_{\rm I}\sinh\delta}\left\{-\rho_{\rm NM'}l_{\rm NM'}j_{s,{\rm NM'}}(z_{\rm I})\cosh\delta + \rho_{\rm NM}l_{\rm NM}\left[\pm{\rm csch}\left(\frac{z_{\rm I}}{l_{\rm NM}}\right) - j_{s,{\rm NM}}(z_{\rm I}){\rm coth}\left(\frac{z_{\rm I}}{l_{\rm NM}}\right)\right]\right\}. \tag{A13b}$$

Eliminating $\rho_{\rm NM}l_{\rm NM}$ from the above two equations, we obtain

$$\frac{j_{s,{\rm NM}}(z_{\rm I})}{j_{s,{\rm NM'}}(z_{\rm I})} = \cosh\delta + \frac{\rho_{\rm NM'}l_{\rm NM'}}{AR_{\rm I}}\delta\sinh\delta, \tag{A14}$$

and reproduce Eq. (8) in Sec. II B.

Pt|Py bilayer

To examine the validity of extracting the SML δ and interface polarization γ for a NM|FM interface with a fully polarized current injected from the NM side, we take Pt|Py as an example and compare the numerical results we find with those obtained by passing an unpolarized current through a NM|FM|NM trilayer structure [51,56]. We construct a diffusive Pt(10 nm)|Py(15 nm) bilayer at room temperature with thermal lattice and spin disorder. The lattice mismatch between the two fcc metals is accommodated using a $2\sqrt{13} \times 2\sqrt{13}$ supercell of (111) oriented Pt matched to a 8×8 supercell of (111) Py. The bilayer is then sandwiched between Cu leads whose lattice constant is chosen to be the same as that of Py. The minority-spin (or majority-spin) potential of Cu in the left lead is artificially increased by 1 Rydberg so all the incoming Bloch states have pure spin character and the charge current injected from the left Cu lead is fully spin polarized. In the transport calculation, the 2D Brillouin zone of the matched lateral supercell is sampled using a 28×28 k-mesh corresponding to a 224×224 sampling of a unit cell of fcc Py. The results we show are obtained by averaging over 20 random configurations of thermally disordered Pt|Py bilayers. Note that the Py is sufficiently thick that the right-hand lead does not affect j_s at the Pt|Py interface plotted in Fig. 10.

The plane-averaged spin current $j_s(z)$ we obtain for the Pt|Py bilayer is shown in Fig. 10. Using Eq. (A2), it can be fitted piecewise in Pt (solid lines) and in Py (dashed lines) and the values required at the interface are obtained by extrapolating these fits. On injecting a spin current with positive polarization into Pt, $j_s(-\infty) = 1$ (blue symbols and lines), we find $j_s(z_{\rm I} - \eta) = 0.28 \pm 0.01$ and $j_s(z_{\rm I} + \eta) = 0.39 \pm 0.01$ by extrapolation. Substituting these values into Eqs. (A12a) and (A12b) together with the independently determined bulk parameters, $\rho_{\rm Pt} = 10.7 \pm 0.03\,\mu\Omega\,{\rm cm}$, $l_{\rm Pt} = 5.25 \pm 0.03$ nm, $\rho_{\rm Py} = 15.6 \pm 0.02\,\mu\Omega\,{\rm cm}$, $l_{\rm Py} = 2.85 \pm 0.02$ nm, and $AR_{\rm Pt|Py} = 0.79 \pm 0.03\,{\rm f}\Omega\,{\rm m}^2$, we finally obtain $\delta = 0.65 \pm 0.14$ and $\gamma = -0.03 \pm 0.06$. Injecting a spin current with negative polarization, $j_s(-\infty) = -1$ (red symbols and lines), we find $j_s(z_{\rm I} - \eta) = 0.17 \pm 0.01$ and $j_s(z_{\rm I} + \eta) = 0.34 \pm 0.01$, yielding $\delta = 0.63 \pm 0.08$ and $\gamma = -0.03 \pm 0.07$. These values are consistent with the values calculated using the Pt|Py|Pt trilayer structure $\delta = 0.76 \pm 0.11$ and $\gamma = -0.06 \pm 0.09$ within the error bars of the calculations [51,56].

[1] M. N. Baibich, J. M. Broto, A. Fert, F. Nguyen Van Dau, F. Petroff, P. Etienne, G. Creuzet, A. Friederich, and J. Chazelas, Giant Magnetoresistance of (001)Fe/(001)Cr Magnetic Superlattices, Phys. Rev. Lett. **61**, 2472 (1988).

[2] G. Binasch, P. Grünberg, F. Saurenbach, and W. Zinn, Enhanced magnetoresistance in layered magnetic structures with antiferromaganetic interlayer exchange, Phys. Rev. B **39**, 4828 (1989).

[3] S. S. P. Parkin, Origin of Enhanced Magnetoresistance of Magnetic Multilayers: Spin-Dependent Scattering from Magnetic Interface States, Phys. Rev. Lett. **71**, 1641 (1993).

[4] J. C. Slonczewski, Current-driven excitation of magnetic multilayers, J. Magn. Magn. Mater. **159**, L1 (1996).

[5] L. Berger, Emission of spin waves by a magnetic multilayer traversed by a current, Phys. Rev. B **54**, 9353 (1996).

[6] M. Tsoi, A. G. M. Jansen, J. Bass, W.-C. Chiang, M. Seck, V. Tsoi, and P. Wyder, Excitation of a Magnetic Multilayer by an Electric Current, Phys. Rev. Lett. **80**, 4281 (1998).

[7] X. Waintal, E. B. Myers, P. W. Brouwer, and D. C. Ralph, Role of spin-dependent interface scattering in generating current-induced torques in magnetic multilayers, Phys. Rev. B **62**, 12317 (2000).

[8] K. Xia, P. J. Kelly, G. E. W. Bauer, A. Brataas, and I. Turek, Spin torques in ferromagnetic/normal-metal structures, Phys. Rev. B **65**, 220401(R) (2002).

[9] M. D. Stiles and A. Zangwill, Anatomy of spin-transfer torque, Phys. Rev. B **66**, 014407 (2002); D. C. Ralph and M. D. Stiles, Spin transfer torques, J. Magn. Magn. Mater. **320**, 1190 (2008).

[10] A. Brataas, G. E. W. Bauer, and P. J. Kelly, Non-collinear magnetoelectronics, Phys. Rep. **427**, 157 (2006).

[11] Q. Shao, P. Li, L. Liu, H. Yang, S. Fukami, A. Razavi, H. Wu, K. Wang, F. Freimuth, Y. Mokrousov, M. D. Stiles, S. Emori, A. Hoffmann, J. Åkerman, K. Roy, J.-P. Wang, S.-H. Yang, K. Garello, and W. Zhang, Roadmap of spin-orbit torques, IEEE Trans. Magn. **57**, 800439 (2021).

[12] M. I. Dyakonov and V. I. Perel, Current-induced spin orientation of electrons in semiconductors, Phys. Lett. A **35**, 459 (1971).

[13] J. E. Hirsch, Spin Hall Effect, Phys. Rev. Lett. **83**, 1834 (1999).

[14] S. Zhang, Spin Hall Effect in the Presence of Spin Diffusion, Phys. Rev. Lett. **85**, 393 (2000).

[15] K. Ando, S. Takahashi, K. Harii, K. Sasage, J. Ieda, S. Maekawa, and E. Saitoh, Electric Manipulation of Spin Relaxation Using the Spin Hall Effect, Phys. Rev. Lett. **101**, 036601 (2008).

[16] L. Liu, R. A. Buhrman, and D. C. Ralph, Review and analysis of measurements of the spin Hall effect in platinum, arXiv:1111.3702.

[17] A. Hoffmann, Spin Hall effects in metals, IEEE Trans. Magn. **49**, 5172 (2013).

[18] J. Sinova, S. O. Valenzuela, J. Wunderlich, C. H. Back, and T. Jungwirth, Spin Hall effects, Rev. Mod. Phys. **87**, 1213 (2015).

[19] Y. Tserkovnyak, A. Brataas, and G. E. W. Bauer, Enhanced Gilbert damping in thin ferromagnetic films, Phys. Rev. Lett. **88**, 117601 (2002); Spin pumping and magnetization dynamics in metallic multilayers, Phys. Rev. B **66**, 224403 (2002); Y. Tserkovnyak, A. Brataas, G. E. W. Bauer, and B. I. Halperin, Nonlocal magnetization dynamics in ferromagnetic nanostructures, Rev. Mod. Phys. **77**, 1375 (2005).

[20] E. Saitoh, M. Ueda, H. Miyajima, and G. Tatara, Conversion of spin current into charge current at room temperature: Inverse spin-Hall effect, Appl. Phys. Lett. **88**, 182509 (2006).

[21] K. Ando, Y. Kajiwara, S. Takahashi, S. Maekawa, K. Takemoto, M. Takatsu, and E. Saitoh, Angular dependence of inverse spin-Hall effect induced by spin pumping investigated in a $Ni_{81}Fe_{19}$ thin film, Phys. Rev. B **78**, 014413 (2008).

[22] O. Mosendz, J. E. Pearson, F. Y. Fradin, G. E. W. Bauer, S. D. Bader, and A. Hoffmann, Quantifying Spin Hall Angles from Spin Pumping: Experiments and Theory, Phys. Rev. Lett. **104**, 046601 (2010).

[23] A. Azevedo, L. H. Vilela-Leão, R. L. Rodríguez-Suárez, A. F. Lacerda Santos, and S. M. Rezende, Spin pumping and anisotropic magnetoresistance voltages in magnetic bilayers: Theory and experiment, Phys. Rev. B **83**, 144402 (2011).

[24] J.-C. Rojas-Sánchez, N. Reyren, P. Laczkowski, W. Savero, J.-P. Attané, C. Deranlot, M. Jamet, J.-M. George, L. Vila, and H. Jaffrès, Spin Pumping and Inverse Spin Hall Effect in Platinum: The Essential Role of Spin-Memory Loss at Metallic Interfaces, Phys. Rev. Lett. **112**, 106602 (2014).

[25] X. Tao, Q. Liu, B. Miao, R. Yu, Z. Feng, L. Sun, B. You, J. Du, K. Chen, S. Zhang, L. Zhang, Z. Yuan, D. Wu, and H. Ding, Self-consistent determination of spin Hall angle and spin diffusion length in Pt and Pd: The role of the interface spin loss, Sci. Adv. **4**, eaat1670 (2018).

[26] K. Uchida, J. Xiao, H. Adachi, J. Ohe, S. Takahashi, J. Ieda, T. Ota, Y. Kajiwara, H. Umezawa, H. Kawai, G. E. W. Bauer, S. Maekawa, and E. Saitoh, Spin Seebeck insulator, Nat. Mater. **9**, 894 (2010).

[27] J. Xiao, G. E. W. Bauer, K.-C. Uchida, E. Saitoh, and S. Maekawa, Theory of magnon-driven spin Seebeck effect, Phys. Rev. B **81**, 214418 (2010).

[28] E.-J. Guo, J. Cramer, A. Kehlberger, C. A. Ferguson, D. A. MacLaren, G. Jakob, and M. Kläui, Influence of Thickness and Interface on the Low-Temperature Enhancement of the Spin Seebeck Effect in YIG Films, Phys. Rev. X **6**, 031012 (2016).

[29] A. Fert and S.-F. Lee, Theory of the bipolar spin switch, Phys. Rev. B **53**, 6554 (1996).

[30] D. V. Baxter, S. D. Steenwyk, J. Bass, and W. P. Pratt, Jr., Resistance and spin-direction memory loss at Nb/Cu interfaces, J. Appl. Phys. **85**, 4545 (1999).

[31] H. Kurt, R. Loloee, K. Eid, W. P. Pratt, Jr., and J. Bass, Spin-memory loss at 4.2 K in sputtered Pd and Pt and at Pd/Cu and Pt/Cu interfaces, Appl. Phys. Lett. **81**, 4787 (2002).

[32] K. Eid, D. Portner, J. A. Borchers, R. Loloee, M. A. Darwish, M. Tsoi, R. D. Slater, K. V. O'Donovan, H. Kurt, W. P. Pratt, Jr., and J. Bass, Absence of mean-free-path effects in the current-perpendicular-to-plane magnetoresistance of magnetic multilayers, Phys. Rev. B **65**, 054424 (2002).

[33] J. Bass and W. P. Pratt, Jr., Spin-diffusion lengths in metals and alloys, and spin-flipping at metal/metal interfaces: An experimentalist's critical review, J. Phys.: Condens. Matter **19**, 183201 (2007).

[34] M. Isasa, E. Villamor, L. E. Hueso, M. Gradhand, and F. Casanova, Temperature dependence of spin diffusion length and spin Hall angle in Au and Pt, Phys. Rev. B **91**, 024402 (2015).

[35] M. Isasa, E. Villamor, L. E. Hueso, M. Gradhand, and F. Casanova, Erratum: Temperature dependence of spin diffusion length and spin Hall angle in Au and Pt [Phys. Rev. B 91, 024402 (2015)], Phys. Rev. B **92**, 019905(E) (2015).

[36] M. H. Nguyen, D. C. Ralph, and R. A. Buhrman, Spin Torque Study of the Spin Hall Conductivity and Spin Diffusion Length in Platinum thin Films with Varying Resistivity, Phys. Rev. Lett. **116**, 126601 (2016).

[37] E. Sagasta, Y. Omori, M. Isasa, M. Gradhand, L. E. Hueso, Y. Niimi, Y. C. Otani, and F. Casanova, Tuning the spin Hall

effect of Pt from the moderately dirty to the superclean regime, Phys. Rev. B **94**, 060412(R) (2016).

[38] C. Swindells, A. T. Hindmarch, A. J. Gallant, and D. Atkinson, Spin transport across the interface in ferromagnetic/nonmagnetic systems, Phys. Rev. B **99**, 064406 (2019).

[39] L. Zhu, D. C. Ralph, and R. A. Buhrman, Maximizing spin-orbit torque generated by the spin Hall effect of Pt, Appl. Phys. Rev. **8**, 031308 (2021).

[40] Y. Liu, Z. Yuan, R. J. H. Wesselink, A. A. Starikov, and P. J. Kelly, Interface Enhancement of Gilbert Damping from First Principles, Phys. Rev. Lett. **113**, 207202 (2014).

[41] K. Chen and S. Zhang, Spin Pumping in the Presence of Spin-Orbit Coupling, Phys. Rev. Lett. **114**, 126602 (2015).

[42] R. J. H. Wesselink, K. Gupta, Z. Yuan, and P. J. Kelly, Calculating spin transport properties from first principles: Spin currents, Phys. Rev. B **99**, 144409 (2019).

[43] T. Valet and A. Fert, Theory of the perpendicular magnetoresistance in magnetic multilayers, Phys. Rev. B **48**, 7099 (1993).

[44] M. A. M. Gijs, S. K. J. Lenczowski, and J. B. Giesbers, Perpendicular Giant Magnetoresistance of Microstructured Fe/Cr Magnetic Multilayers from 4.2 to 300 K, Phys. Rev. Lett. **70**, 3343 (1993); M. A. M. Gijs and G. E. W. Bauer, Perpendicular giant magnetoresistance of magnetic multilayers, Adv. Phys. **46**, 285 (1997).

[45] W. P. Pratt, Jr., S.-F. Lee, J. M. Slaughter, R. Loloee, P. A. Schroeder, and J. Bass, Perpendicular Giant Magnetoresistance of Ag/Co Multilayers, Phys. Rev. Lett. **66**, 3060 (1991); J. Bass and W. P. Pratt, Jr., Current-perpendicular (CPP) magnetoresistance in magnetic metallic multilayers, J. Magn. Magn. Mater. **200**, 274 (1999).

[46] K. Xia, P. J. Kelly, G. E. W. Bauer, I. Turek, J. Kudrnovský, and V. Drchal, Interface resistance of disordered magnetic multilayers, Phys. Rev. B **63**, 064407 (2001).

[47] K. Xia, P. J. Kelly, G. E. W. Bauer, and I. Turek, Spin-Dependent Transparency of Ferromagnet/Superconductor Interfaces, Phys. Rev. Lett. **89**, 166603 (2002).

[48] P. X. Xu, K. Xia, M. Zwierzycki, M. Talanana, and P. J. Kelly, Orientation-Dependent Transparency of Metallic Interfaces, Phys. Rev. Lett. **96**, 176602 (2006).

[49] K. Xia, M. Zwierzycki, M. Talanana, P. J. Kelly, and G. E. W. Bauer, First-principles scattering matrices for spin-transport, Phys. Rev. B **73**, 064420 (2006).

[50] Y. Liu, A. A. Starikov, Z. Yuan, and P. J. Kelly, First-principles calculations of magnetization relaxation in pure Fe, Co, and Ni with frozen thermal lattice disorder, Phys. Rev. B **84**, 014412 (2011); Y. Liu, Z. Yuan, R. J. H. Wesselink, A. A. Starikov, M. van Schilfgaarde, and P. J. Kelly, Direct method for calculating temperature-dependent transport properties, *ibid.* **91**, 220405(R) (2015).

[51] K. Gupta, R. J. H. Wesselink, R. Liu, Z. Yuan, and P. J. Kelly, Disorder Dependence of Interface Spin Memory Loss, Phys. Rev. Lett. **124**, 087702 (2020).

[52] K. D. Belashchenko, A. A. Kovalev, and M. van Schilfgaarde, Theory of Spin Loss at Metallic Interfaces, Phys. Rev. Lett. **117**, 207204 (2016).

[53] G. G. Baez Flores, A. A. Kovalev, M. van Schilfgaarde, and K. D. Belashchenko, Generalized magnetoelectronic circuit theory and spin relaxation at interfaces in magnetic multilayers, Phys. Rev. B **101**, 224405 (2020).

[54] K. Dolui and B. K. Nikolić, Spin-memory loss due to spin-orbit coupling at ferromagnet/heavy-metal interfaces: Ab initio spin-density matrix approach, Phys. Rev. B **96**, 220403(R) (2017).

[55] M. Lim and H.-W. Lee, Spin-memory loss induced by bulk spin orbit coupling at ferromagnet/heavy-metal interfaces, Appl. Phys. Lett. **118**, 042408 (2021).

[56] K. Gupta, R. J. H. Wesselink, Z. Yuan, and P. J. Kelly, Spin transport at finite temperatures: A first-principles study for ferromagnetic|nonmagnetic interfaces, Phys. Rev. B **104**, 205426 (2021).

[57] O. Gunnarsson, Band model for magnetism of transition metals in the spin-density-functional formalism, J. Phys. F: Met. Phys. **6**, 587 (1976).

[58] J. F. Janak, Uniform susceptibilities of metallic elements, Phys. Rev. B **16**, 255 (1977).

[59] S. Y. Huang, X. Fan, D. Qu, Y. P. Chen, W. G. Wang, J. Wu, T. Y. Chen, J. Q. Xiao, and C. L. Chien, Transport Magnetic Proximity Effects in Platinum, Phys. Rev. Lett. **109**, 107204 (2012).

[60] D. Qu, S. Y. Huang, J. Hu, R. Wu, and C. L. Chien, Intrinsic Spin Seebeck Effect in Au/YIG, Phys. Rev. Lett. **110**, 067206 (2013).

[61] H. Nakayama, M. Althammer, Y.-T. Chen, K. Uchida, Y. Kajiwara, D. Kikuchi, T. Ohtani, S. Geprägs, M. Opel, S. Takahashi, R. Gross, G. E. W. Bauer, S. T. B. Goennenwein, and E. Saitoh, Spin Hall magnetoresistance induced by a nonequilibrium proximity effect, Phys. Rev. Lett. **110**, 206601 (2013).

[62] M. Caminale, A. Ghosh, S. Auffret, U. Ebels, K. Ollefs, F. Wilhelm, A. Rogalev, and W. E. Bailey, Spin pumping damping and magnetic proximity effect in Pd and Pt spin-sink layers, Phys. Rev. B **94**, 014414 (2016).

[63] S. Emori, A. Matyushov, H.-M. Jeon, C. J. Babroski, T. Nan, A. M. Belkessam, J. G. Jones, M. E. McConney, G. J. Brown, B. M. Howe, and N. X. Sun, Spin-orbit torque and spin pumping in YIG/Pt with interfacial insertion layers, Appl. Phys. Lett. **112**, 182406 (2018).

[64] F. J. Jedema, A. T. Filip, and B. J. van Wees, Electrical spin injection and accumulation at room temperature in an all-metal mesoscopic spin valve, Nature (London) **410**, 345 (2001).

[65] T. Kimura, Y. Otani, T. Sato, S. Takahashi, and S. Maekawa, Room-Temperature Reversible Spin Hall Effect, Phys. Rev. Lett. **98**, 156601 (2007).

[66] L. Vila, T. Kimura, and Y. C. Otani, Evolution of the Spin Hall Effect in Pt Nanowires: Size and Temperature Effects, Phys. Rev. Lett. **99**, 226604 (2007).

[67] Y. Niimi, D. Wei, H. Idzuchi, T. Wakamura, T. Kato, and Y. C. Otani, Experimental Verification of Comparability between Spin-Orbit and Spin-Diffusion Lengths, Phys. Rev. Lett. **110**, 016805 (2013).

[68] C. Zhou, F. Kandaz, Y. Cai, C. Qin, M. Jia, Z. Yuan, Y. Wu, and Y. Ji, Anisotropic spin relaxation induced by surface spin-orbit effects, Phys. Rev. B **96**, 094413 (2017).

[69] Y. Omori, E. Sagasta, Y. Niimi, M. Gradhand, L. E. Hueso, F. Casanova, and Y. C. Otani, Relation between spin Hall effect and anomalous Hall effect in 3*d* ferromagnetic metals, Phys. Rev. B **99**, 014403 (2019).

[70] A. A. Starikov, P. J. Kelly, A. Brataas, Y. Tserkovnyak, and G. E. W. Bauer, Unified First-Principles Study of Gilbert

Damping, Spin-Flip Diffusion and Resistivity in Transition Metal Alloys, Phys. Rev. Lett. **105**, 236601 (2010); A. A. Starikov, Y. Liu, Z. Yuan, and P. J. Kelly, Calculating the transport properties of magnetic materials from first-principles including thermal and alloy disorder, non-collinearity and spin-orbit coupling, Phys. Rev. B **97**, 214415 (2018).

[71] Z. Yuan, Y. Liu, A. A. Starikov, P. J. Kelly, and A. Brataas, Spin-orbit-coupling-induced domain-wall resistance in diffusive ferromagnets, Phys. Rev. Lett. **109**, 267201 (2012); Z. Yuan, K. M. D. Hals, Y. Liu, A. A. Starikov, A. Brataas, and P. J. Kelly, Gilbert damping in noncollinear ferromagnets, *ibid.* **113**, 266603 (2014).

[72] J. Stöhr and H. C. Siegmann, *Magnetism: From Fundamentals to Nanoscale Dynamics*, edited by M. Carona, P. Fulde, K. von Klitzing, R. Merlin, H.-J. Queisser, and H. Störmer, Springer Series in Solid-State Sciences, Vol. 152 (Springer, Berlin, 2006).

[73] J. Bass, CPP magnetoresistance of magnetic multilayers: A critical review, J. Magn. Magn. Mater. **408**, 244 (2016).

[74] K. Gupta, R. J. H. Wesselink, R. Liu, Z. Yuan, and P. J. Kelly, Calculating interface transport parameters at finite temperatures: Nonmagnetic interfaces, (unpublished).

[75] P. Hohenberg and W. Kohn, Inhomogeneous electron gas, Phys. Rev. **136**, B864 (1964).

[76] W. Kohn and L. J. Sham, Self-consistent equations including exchange and correlation effects, Phys. Rev. **140**, A1133 (1965).

[77] O. K. Andersen and O. Jepsen, Explicit, First-Principles Tight-Binding Theory, Phys. Rev. Lett. **53**, 2571 (1984); O. K. Andersen, O. Jepsen, and D. Glötzel, Canonical description of the band structures of metals, in Highlights of Condensed Matter Theory, in *Proceedings of the International School of Physics 'Enrico Fermi', Varenna, Italy*, edited by F. Bassani, F. Fumi, and M. P. Tosi (North-Holland, Amsterdam, 1985), pp. 59–176; O. K. Andersen, Z. Pawlowska, and O. Jepsen, Illustration of the linear-muffin-tin-orbital tight-binding representation: Compact orbitals and charge density in Si, Phys. Rev. B **34**, 5253 (1986).

[78] O. K. Andersen, Linear methods in band theory, Phys. Rev. B **12**, 3060 (1975).

[79] U. von Barth and L. Hedin, A local exchange-correlation potential for the spin-polarized case: I, J. Phys. C: Solid State Phys. **5**, 1629 (1972).

[80] T. Ando, Quantum point contacts in magnetic fields, Phys. Rev. B **44**, 8017 (1991).

[81] M. Zwierzycki, P. A. Khomyakov, A. A. Starikov, K. Xia, M. Talanana, P. X. Xu, V. M. Karpan, I. Marushchenko, I. Turek, G. E. W. Bauer, G. Brocks, and P. J. Kelly, Calculating scattering matrices by wave function matching, Phys. Status Solidi B **245**, 623 (2008).

[82] S. Datta, *Electronic Transport in Mesoscopic Systems* (Cambridge University Press, Cambridge, 1995).

[83] L. Wang, R. J. H. Wesselink, Y. Liu, Z. Yuan, K. Xia, and P. J. Kelly, Giant Room Temperature Interface Spin Hall and Inverse Spin Hall Effects, Phys. Rev. Lett. **116**, 196602 (2016).

[84] H. Ibach and H. Lüth, *Solid-State Physics*, 2nd ed. (Springer-Verlag, Berlin, 1995).

[85] K. Gupta, Disentangling interfaces and bulk in spin transport calculations, Ph.D. thesis, University of Twente, The Netherlands, 2019.

[86] P. Soven, Coherent-potential model of substitutional disordered alloys, Phys. Rev. **156**, 809 (1967).

[87] I. Turek, V. Drchal, J. Kudrnovský, M. Šob, and P. Weinberger, *Electronic Structure of Disordered Alloys, Surfaces and Interfaces* (Kluwer, Boston-London-Dordrecht, 1997).

[88] L. Yang, T. S. Rahman, and M. S. Daw, Surface vibrations of Ag(100) and Cu(100): A molecular-dynamics study, Phys. Rev. B **44**, 13725 (1991).

[89] O. Mironets, H. L. Meyerheim, C. Tusche, P. Zschack, H. Hong, N. Jeutter, R. Felici, and J. Kirschner, Surface vibrations and relaxation effects in cu(001) studied by x-ray diffraction, Phys. Rev. B **78**, 153401 (2008).

[90] R. Fisher, Dispersion on a sphere, Proc. Roy. Soc. A **217**, 295 (1953).

[91] R. S. Nair, E. Barati, K. Gupta, Z. Yuan, and P. J. Kelly, Spin-Flip Diffusion Length in 5*d* Transition Metal Elements: A First-Principles Benchmark, Phys. Rev. Lett. **126**, 196601 (2021).

[92] R. J. Elliott, Theory of the effect of spin-orbit coupling on magnetic resonance in some semiconductors, Phys. Rev. **96**, 266 (1954).

[93] Y. Yafet, g factors and spin-lattice relaxation of conduction electrons, in *Solid State Physics*, edited by F. Seitz and D. Turnbull (Academic, New York, 1963), Vol. 14, pp. 1–98.

[94] Y. Imry, *Introduction to Mesoscopic Physics*, 2nd ed. (Oxford University Press, Oxford, 2002).

[95] An explicit numerical check showed that $L_{\mathrm{Cu}} = 10\,\mathrm{nm}$ is enough to reproduce the linear dependence of the resistance on the Cu length and therefore a longer L_{Cu} would not alter the final value of the SML that we are interested in.

[96] R. Freeman, A. Zholud, Z. Dun, H. Zhou, and S. Urazhdin, Evidence for Dyakonov-Perel-Like Spin Relaxation in Pt, Phys. Rev. Lett. **120**, 067204 (2018).

[97] B. Doudin, A. Blondel, and J.-Ph. Ansermet, Arrays of multilayered nanowires, J. Appl. Phys. **79**, 6090 (1996).

[98] Y. Ji, A. Hoffmann, J. E. Pearson, and S. D. Bader, Enhanced spin injection polarization in Co/Cu/Co nonlocal lateral spin valves, Appl. Phys. Lett. **88**, 052509 (2006).

[99] F. J. Albert, N. C. Emley, E. B. Myers, D. C. Ralph, and R. A. Buhrman, Quantitative Study of Magnetization Reversal by Spin-Polarized Current in Magnetic Multilayer Nanopillars, Phys. Rev. Lett. **89**, 226802 (2002).

[100] F. J. Jedema, M. S. Nijboer, A. T. Filip, and B. J. van Wees, Spin injection and spin accumulation in all-metal mesoscopic spin valves, Phys. Rev. B **67**, 085319 (2003).

[101] T. Kimura, J. Hamrle, and Y. Otani, Estimation of spin-diffusion length from the magnitude of spin-current absorption: Multiterminal ferromagnetic/nonferromagnetic hybrid structures, Phys. Rev. B **72**, 014461 (2005).

[102] S. Maekawa, ed., *Concepts in Spin Electronics* (Oxford University Press, Oxford, 2006).

[103] B. Dassonneville, R. Acharyya, H. Y. T. Nguyen, R. Loloee, W. P. Pratt, Jr., and J. Bass, A way to measure electron spin-flipping at ferromagnetic/nonmagnetic interfaces and application to Co/Cu, Appl. Phys. Lett. **96**, 022509 (2010).

[104] L. Zhu, L. Zhu, and R. A. Buhrman, Fully Spin-Transparent Magnetic Interfaces Enabled by the Insertion of a Thin Paramagnetic NiO Layer, Phys. Rev. Lett. **126**, 107204 (2021).